Zeitschrift: IABSE congress report = Rapport du congrès AIPC = IVBH Kongressbericht

Band: 13 (1988)

Rubrik: III. Special topics in design and analysis

SEMINAR

III

Special Topics in Design and Analysis

Sujets particuliers dans le projet et le calcul des structures

Spezielle Themen in Entwurf und Berechnungen von Tragwerken

Chairman: R. Sormunen, Finland

Technical Adviser: J. Schneider, Switzerland

Leere Seite
Blank page
Page vide

Modelling the Fire Behaviour of Multistorey Buildings

Modélisation du comportement au feu de bâtiments à étages multiples

Modellierung des Brandverhaltens von mehrgeschossigen Gebäuden

Reijo KOUHIA
Research Scientist
Finnish Academy
Espoo, Finland

Juha PAAVOLA
Research Scientist
Helsinki Univ. of Techn.
Espoo, Finland

Markku TUOMALA
Professor
Tampere Univ. of Techn.
Tampere, Finland

SUMMARY
A finite element method is developed for steel framed structures subjected to large loads and high temperatures. Material nonlinearities and large deformations are taken into account. An incremental Lagrangian description is adopted in formulating the equations of motion of structures. An elastic plastic material model within a theory of plasticity is formulated based on the recent studies on the properties of steel at temperatures 20–600°C. An incremental iterative procedure is established to follow the nonlinear response of structures. Emphasis is given to detecting the onset of local nonlinearities, their progress and interaction with global structural response. Beams and frames exposed to fire are analyzed and results are compared with experimental data.

RÉSUMÉ
Une méthode des éléments finis a été développée pour l'analyse des portiques en acier, soumis aux grandes charges et aux hautes températures. Les matériaux déformés du modèle ainsi que les grandes déformations sont pris en compte. Une équation de Lagrange a été adoptée afin d'établir les équations de mouvements des structures. Les récentes études sur les propriétés des aciers soumis aux températures de 20 à 600°C ont permis de formuler un modèle élasto-plastique selon la théorie de la plasticité. Une méthode itérative a été établie pour suivre la réaction non linéaire des structures. L'accent a été mis sur la détection des apparitions de déformées locales sur leur interaction avec la réaction structurale globale. Des poutres et des portiques exposés au feu ont été analysés. Les résultats ont été comparés avec des données expérimentales.

ZUSAMMENFASSUNG
Ein Finite-Element-Verfahren für Stahlrahmentragwerke bei grossen Lasten und hohen Temperaturen wurde entwickelt, bei dem Materialnichtlinearitäten und grosse Deformationen berücksichtigt werden. Die Bewegungsgleichungen basieren auf der inkrementellen Lagrangeformulierung. Eiun elastoplastisches Materialgesetz auf der Grundlage einer Plastisitätstheorie, das sich auf neueste Ergebnisse der Materialforschungen an Stahl bis 600°C stützt, wurde erarbeitet. Das Modell zur Berechnung des nichtlinearen Strukturverhaltens verwendet ein inkrementelles Iterationsverfahren. Der Beginn lokaler Nichtlinearität, ihr Fortschreiten und ihr Zusammenwirken mit der Gesamtstruktur wird besonders beachtet. Die Rechenergebnisse brandbeanspruchter Balken und Rahmen werden mit Versuchsergebnissen verglichen.

1. INTRODUCTION

The behaviour of structures under large loads and high temperatures is complex due to material nonlinearities and large deformations. In fire safety analysis of steel structures analytical calculation methods are applicable only for very simple structures with considerable approximations in the analysing model. Detailed information about structural behaviour can be obtained by the finite element method, FEM. Linear elastic analyses by FEM are nowadays a part of everyday practice in engineering design. In many important applications, however, they do not provide information enough for completely safe but economical design. Nonlinear FEM analyses, on the contrary, require much more experience from the user because material and geometrical nonlinearities are coupled. However, the character of the load-deformation curve is important in assessing the safety of the structure in the post-buckling range.

In the present study a geometrically nonlinear elasto-plastic finite element analysis of steel frames in high temperatures is considered. Finite deformations are taken into account by adopting an incremental Lagrangian formulation of the problem. The temperature dependence of material parameters is modelled in accordance with Refs. [1,2]. The resulting nonlinear equilibrium equations are solved by an incremental iterative procedure based on Newton's method. In constant temperature analyses an arc-length method is used. In transient problems creep type displacement-temperature curves are integrated by an adaptive step-size selection method. The FEM program developed is applicable for three-dimensional beams and frames.

The numerical examples calculated consist of steel beams and frames for which experimental data exist. Solutions obtained by different material models are compared with the test results of Refs. [2,4]. In addition, an ECCS calibrating multistorey frame [3] exposed to a local fire is studied.

2. FINITE ELEMENT FORMULATION

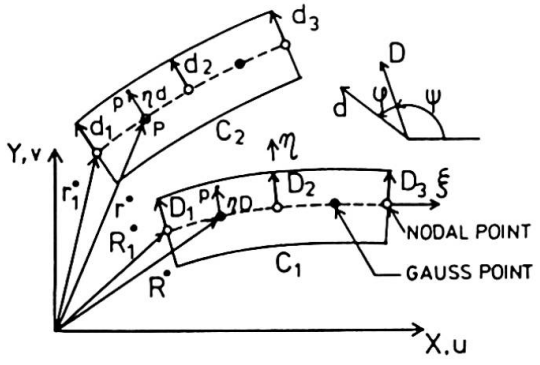

Fig. 1 Geometry of plane frame element

In the finite element method the displacement vector $\mathbf{u}$ of a material point $\mathbf{X}$ is interpolated within an element by shape functions $\mathbf{N}$ and nodal point displacements $\mathbf{q}$

$$\mathbf{u}(\mathbf{X}) = \mathbf{N}(\mathbf{X})\mathbf{q} \qquad (1)$$

Inserting (1) into an equation of incremental virtual work gives the following equilibrium equation [5]

$$^1(\mathbf{K}_1 + \mathbf{K}_g)\mathbf{q} = ^2\mathbf{Q} - ^1\mathbf{F} \qquad (2)$$

where $\mathbf{K} = \mathbf{K}_1 + \mathbf{K}_g$ is the tangent stiffness matrix, $\mathbf{K}_g$ the geometrical stiffness matrix, $\mathbf{Q}$ the external force vector and $\mathbf{F}$ the vector of internal forces. The left superscript 1 refers to the reference configuration at $\mathbf{q}(t_i)$ and the index 2 to the configuration at $\mathbf{q}(t_i + \Delta t)$, where t is a load parameter. In the incremental Lagrangian formulation the matrix $\mathbf{K}_1$ is also dependent on incremental deformations between configurations 1 and 2.

An isoparametric curved beam element is shown in Fig. 1. The position vector of an arbitrary point P in the reference configuration is

$$\mathbf{R} = \mathbf{R}^o + \eta \mathbf{D}_1 + \varsigma \mathbf{D}_2 \tag{3}$$

where $\mathbf{D}_k$ are director vectors and η, ς coordinates in the cross section. $\mathbf{R}^o$ and $\mathbf{D}_k$ are interpolated by polynomials N_i

$$\mathbf{R}^o = \sum_{i=1}^{n} N_i(s)\mathbf{R}_i^o, \quad \mathbf{D}_k = \sum_{i=1}^{n} N_i(s)\mathbf{D}_{ki} \tag{4}$$

where n is the number of nodes in one element. In the deformed configuration the position vector of material point P is

$$\mathbf{r} = \mathbf{r}^o + \eta \mathbf{d}_1 + \varsigma \mathbf{d}_2 \tag{5}$$

where $\mathbf{r}^o$ and $\mathbf{d}_k$ are interpolated by polynomials N_i, correspondingly. The director vector $\mathbf{d}$ in the deformed configuration 2 is obtained from $\mathbf{D}$ in configuration 1 by the formula $\mathbf{d} = \mathbf{Q}\mathbf{D}$, in which $\mathbf{Q}$ is a rotation matrix. The displacement vector is then

$$\mathbf{u} = \mathbf{r} - \mathbf{R} \quad or \quad \mathbf{u} = \mathbf{u}^o + \eta(\mathbf{d}_1 - \mathbf{D}_1) + \varsigma(\mathbf{d}_2 - \mathbf{D}_2) \tag{6}$$

where $\mathbf{u}^o$ is the displacement vector of the reference line. The finite element presentation of Eq. (6)

$$\mathbf{u} = \sum N_i(\mathbf{u}_i^o + \eta(\mathbf{d}_1 - \mathbf{D}_1)_i + \varsigma(\mathbf{d}_2 - \mathbf{D}_2)_i) \tag{7}$$

is inserted into an incremental form of the Green-Lagrangian strain tensor

$$E_{ij} = \tfrac{1}{2}(u_{i,j} + u_{j,i} + u_{k,i}u_{k,j}) \tag{8}$$

containing normal strain and shear strains. The stiffness matrices $\mathbf{K}_1$ and $\mathbf{K}_g$ and the vector of internal forces $\mathbf{F}$ for an element are evaluated by numerical integration. In the applications a two-noded element with a one point Gaussian rule [5] is used.

3. CONSTITUTIVE MODEL

The strain rate $\mathbf{D}$ is decomposed into elastic, plastic, creep and thermal parts

$$\mathbf{D} = \mathbf{D}_e + \mathbf{D}_p + \mathbf{D}_c + \mathbf{D}_T \tag{9}$$

The elastic part $\mathbf{D}_e$ is obtained from Hooke's law

$$\boldsymbol{\sigma} = \mathbf{C}\boldsymbol{\epsilon}_e \tag{10}$$

where $\boldsymbol{\sigma}$ is the Cauchy stress tensor, $\mathbf{C}$ an elastic constitutive tensor and $\boldsymbol{\epsilon}_e$ the elastic strain tensor. A rate form of Eq. (10) is

$$\overset{*}{\boldsymbol{\sigma}} = \mathbf{C}\mathbf{D}_e + \frac{\partial \mathbf{C}}{\partial T}\dot{T}\boldsymbol{\epsilon}_e \tag{11}$$

where $\overset{*}{\boldsymbol{\sigma}}$ is the Jaumann rate of $\boldsymbol{\sigma}$. The J_2-flow theory is used to evaluate the plastic strain rate

$$\mathbf{D}_p = \dot{\lambda}\frac{\partial f}{\partial \boldsymbol{\sigma}} \tag{12}$$

where $f = \sqrt{3J_2}$ and J_2 is the second invariant of the deviatoric stress. The thermal strain rate is

$$\mathbf{D}_T = \alpha \dot{T} \mathbf{I} \tag{13}$$

where α is the coefficient of thermal expansion. In short duration loadings $\mathbf{D}_c$ is assumed to vanish. The yield condition is expressed by the formula

$$F = f - \sigma_y = 0 \tag{14}$$

where the yield stress σ_y is dependent on a hardening parameter κ and temperature T. According to the consistency condition during plastic flow

$$dF = \frac{\partial F}{\partial \sigma} d\sigma + \frac{\partial F}{\partial \kappa} d\kappa + \frac{\partial F}{\partial T} dT = 0 \tag{15}$$

By inserting the flow rule Eq. (12) into the equation

$$\overset{*}{\boldsymbol{\sigma}} = \mathbf{C}(\mathbf{D} - \mathbf{D}_p - \mathbf{D}_T) + \frac{\partial \mathbf{C}}{\partial T} \dot{T} \boldsymbol{\epsilon}_e \tag{16}$$

and by using the consistency condition Eq. (15) $\dot{\lambda}$ is obtained [6]. Eq. (16) gives then

$$\overset{*}{\boldsymbol{\sigma}} = (\mathbf{C} - \frac{1}{h}\mathbf{b}\mathbf{b}^T)(\mathbf{D} - \mathbf{D}_T) + \frac{1}{h}\mathbf{b}(\frac{\partial \sigma_y}{\partial T}\dot{T} - \mathbf{a}^T \frac{\partial \mathbf{C}}{\partial T}\dot{T}\boldsymbol{\epsilon}_e) + \frac{\partial \mathbf{C}}{\partial T}\dot{T}\boldsymbol{\epsilon}_e \tag{17}$$

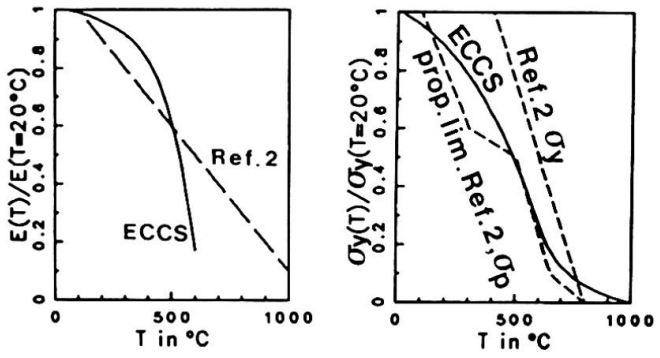

Fig. 2 Modulus of elasticity E and yield stress σ_y vs. temperature

where $\mathbf{a} = \partial f / \partial \sigma$, $\mathbf{b} = \mathbf{C}\mathbf{a}$, $h = \mathbf{a}^T\mathbf{b} + E_p$ and superscript T means transpose. The plastic hardening modulus E_p is obtained from the tangent modulus E_t and the modulus of elasticity E by the formulas

$$E_p = \frac{E E_t}{E - E_t}, \qquad E_t = \frac{d\sigma_y}{d\bar{\epsilon}_p} \tag{18}$$

The yield stress σ_y is obtained from a tension test as a function of the logarithmic inelastic strain

$$\bar{\epsilon}_p = \int \sqrt{\tfrac{2}{3}\mathbf{D}_p \cdot \mathbf{D}_p}\, dt \tag{19}$$

where t is a load parameter. Using the relationship between the strain rate $\mathbf{D}$ and the rate of Green-Lagrange strain $\dot{\mathbf{E}}$ an appropriate constitutive equation for the incremental Lagrangian formulation is obtained in the form

$$\dot{\mathbf{S}} = \mathbf{C}_L \dot{\mathbf{E}} \tag{20}$$

where $\mathbf{S}$ is the 2nd Piola Kirchhoff stress. The temperature dependency of E, σ_y and α is in accordance with Ref. [1] or alternatively with Ref. [2], depicted in Fig. 2. The material model is evaluated at discrete integration points on the cross section. The transverse shear stresses are taken into account.

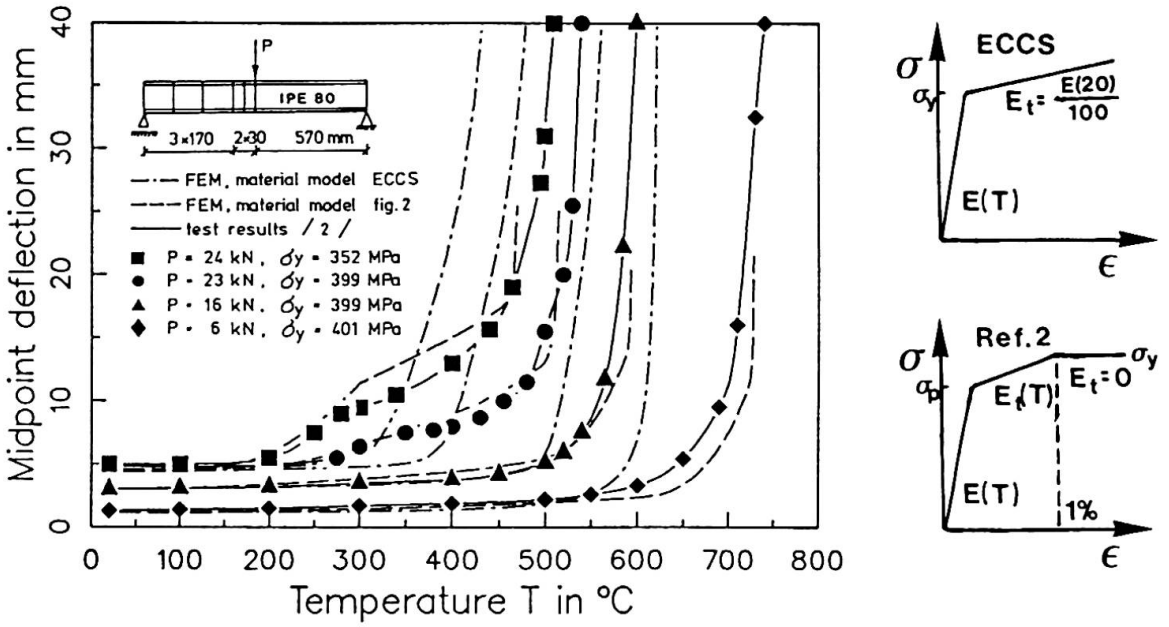

Fig. 3 Central deflection vs. temperature of a beam with various load magnitudes

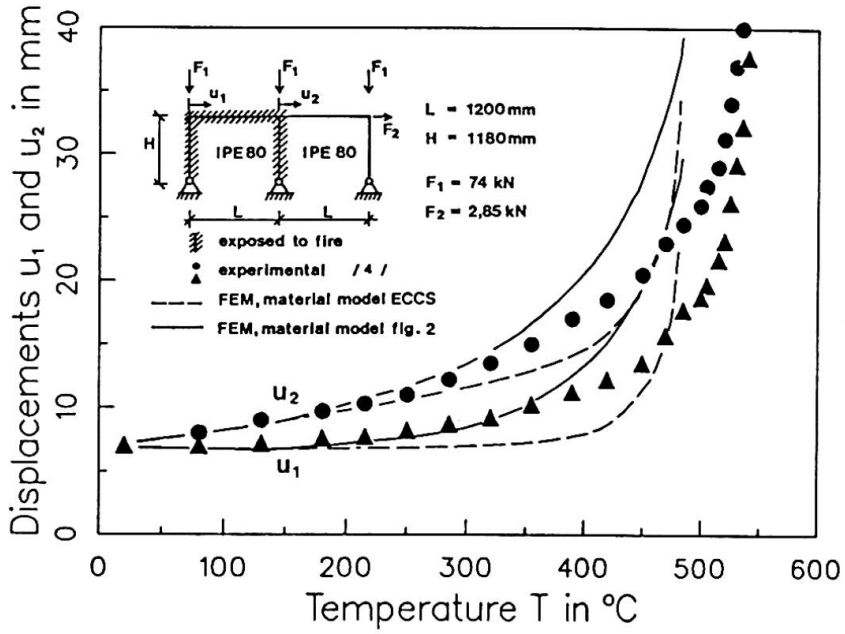

Fig. 4 Horizontal deflections of a two-bay frame

4. APPLICATIONS

Applications are chosen mainly to enable comparisons with experimental data. The FEM program developed is applicable for three-dimensional beams and frames, but, due to the lack of test results on three-dimensional cases, plane structures are analyzed. An IPE 80 beam with a point load at midspan is considered first, merely to verify the material model. The problem definition and the results corresponding to the experimental measurements in [2] are given in Fig. 3. In most cases the ECCS material parameters [1], which are mainly not defined in temperatures over $600°C$, result in conservative estimates for displacements, also under this temperature. The results corresponding to the material parameters of Ref. [2] agree reasonably well with experimental data.

As a second example a two-bay test frame of Ref. [4] is analyzed. The problem definition and the calculated horizontal deflections vs. temperature by using the material parameters of ECCS [1] or Rubert and Schaumann [2] are given in Fig. 4.

Fig. 5 shows the calculated horizontal deflections in the first floor of a multistorey frame (ECCS calibrating frame I in Ref. [3]) and the deformed configurations when exposed to a local fire. The results correspond to ECCS material parameters. Results of a modified frame in which the lower end of the central column is hinged are shown by dashed lines.

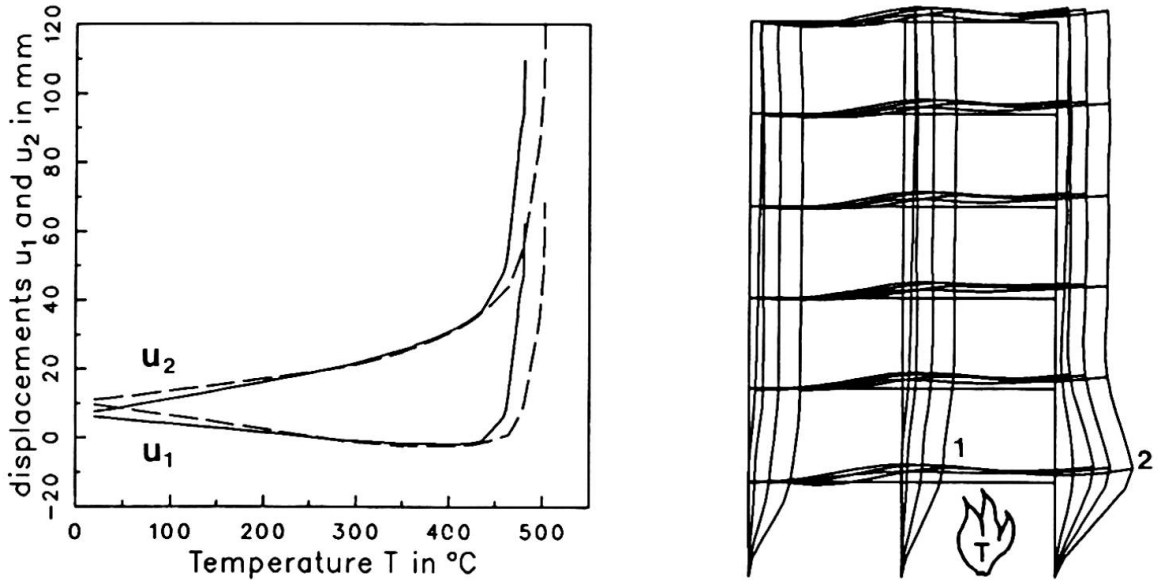

Fig. 5 Horizontal deflections of points 1 and 2 and deformed shapes magnified by a factor of 30 at temperatures 320, 460, 470 and 480°C

REFERENCES

1. European Recommendations for the Fire Safety of Steel Structures. ECCS-Technical Committee 3. Elsevier, 1983.

2. RUBERT A. & SCHAUMANN P., Temperaturabhängige Werkstoffeigenschaften von Baustahl bei Brandbeanspruchung. Stahlbau, 54, 1985, No. 3, 81-86.

3. VOGEL U., Calibrating Frames. Stahlbau, 54, 1985, No.10, 295-301.

4. RUBERT A. & SCHAUMANN P., Tragverhalten stählerner Rahmensysteme bei Brandbeanspruchung. Stahlbau, 54, 1985, No.9, 280-287.

5. ZIENKIEWICZ, O.C., The Finite Element Method. 3 rd edn., Mc Graw-Hill, London 1977, 787 p.

6. HILL R., On the Classical Constitutive Relations for Elastic-Plastic Solids. Recent Progress in Applied Mechanics. Almqvist and Wiksell, Stockholm, 1967, 241-249.

Mathematical Model of Structural Steel Members

Modèle mathématique des éléments structuraux en acier

Ein mathematisches Modell für Stahltragteile

Motoo SAISHO
Assoc. Prof.
Kumamoto University
Kumamoto, Japan

Motoo Saisho, born 1944, received his D.Eng. from the University of Tokyo in 1973. His primary interests are plastic design and numerical analysis of steel buildings. His current research interests include aseismic structures.

SUMMARY
To calculate the restoring force characteristics of steel members under strong loads, a mathematical structural model is proposed in which the idea of "the equivalent two-flange section" is introduced to make it simple. Although the model has only three degrees-of-freedom of end-deformation, the inelastic and hysteretic behavior of steel member can be analyzed by expressing the accumulated plastic deformation in the closed-form function of the end-deformations. From numerical analysis it is pointed out that the presented model is useful and suitable to carry out the analysis of the detailed behavior of steel buildings and it does not require a large amount of calculation to execute it.

RÉSUMÉ
Un modèle structural mathématique est proposé pour calculer les caractéristiques de récupération d'éléments structuraux en acier sous des charges considérables. Le concept de "section à deux semelles équivalentes" est introduit pour la simplification du modèle. Dans ce modèle, il n'y a que trois degrés de liberté de déformations des extrémités, mais les deux comportements d'inélasticité et d'hystérisis des barres en acier peuvent être analysés en exprimant le déformation plastique accumulée dans une fonction de forme fermée des déformations des extrémités. Utilisant une analyse numérique, on a trouvé ce modèle simple, utile et approprié pour l'exécution d'analyses du comportement détaillé de constructions métalliques.

ZUSAMMENFASSUNG
Um die Rückstelleigenschaften von Stahlteilen unter starken Belastungen zu berechnen, wird hier ein mathematisches Strukturmodell vorgestellt, in dem zur Vereinfachung des Modells das Konzept des "gleichwertigen zweiflanschigen Schnitts" eingeführt wird. Das Modell hat nur drei Freiheitsgrade von End-Deformation, aber das inelastische und hysteretische Verhalten von Stahlteilen kann durch die Analyse der angesammelten plastischen Deformationen als eine geschlossene Funktion der End-Deformationen analysiert werden. Verwendet wird eine numerische Analyse, um zu zeigen, dass dieses Modell nützlich und ohne komplizierte Rechnungen anwendbar ist.

1. INTRODUCTION

The collapse of building frames composed of many members is generally caused by local failure or the failure of a few members among many elements of the frame under intense loads such as seismic load or strong wind force. From this reason the behavior of all members must be analyzed accurately in the structural analysis of building frames composed of many members. To calculate the detailed behavior of steel members under strong loads, the following conditions, which change every moment according to the hysteretic behavior, must be satisfied strictly in the analysis.

- The incremental stress-strain relation.
- The accumulated plastic deformation.
- The plastic zone over the cross section and along the axis of steel member.

To execute the above-mentioned analysis, FEM (Finite Element Method) is the best and most widely used analysis method. However, FEM requires a large amount of calculation. Numerical errors in the analysis are accumulated as the amount of calculation increases. For this reason we must try in the numerical analysis to decrease the calculation as much as possible.

The plastic hinge method has been proposed as a simple analysis method of steel members to decrease the amount of calculation.[1]-[5] With this method, it is difficult to calculate the effect of the plastic zone, which changes every moment over the cross section and along the axis of each member.

Another possibility has been presented to decrease the amount of calculation of FEM by introducing a transfer matrix to combine a few elements.[6] In this way, the size of the matrix to be solved in the analysis becomes smaller than that of the original FEM. But this method also requires a large amount of calculation because the number of freedom in the analysis is basically the same as the original FEM.

In this paper a mathematical structural model is presented which is simple but useful in analyzing the behavior of steel members relatively accurately and can be easily applied to the structural analysis of tall buildings.[7]

2. MATHEMATICAL MODEL

2.1 Assumptions

1) The structural model of a steel member is considered with respect to the cantilever member which is subjected to horizontal load (Fx), vertical load (Fz) and bending moment (Fr) at the free end as shown in Fig.1.

2) The section of the steel member is replaced by a two-flange section. The area and the moment inertia of the replaced section are equal to those of the original section in the elastic range.

When plastic strain is generated the section is replaced by "the equivalent two-flange section" explained in the next paragraph.

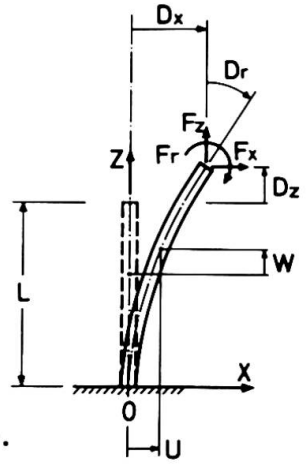

Fig.1
Structural Model

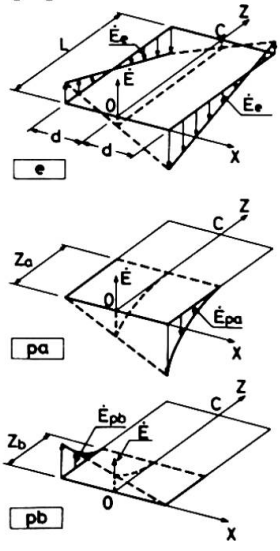

Fig.2
Incremental Strain Distributions

3) The normal stress of the concentrated sections distributes linearly along the axis of the member.

4) The compatibility condition is given by Eq.(1).

$$E=W'+(U')^{**}2/2-U''X \qquad (1)$$

in which E : the normal strain at Z-section, ' : the differentiation with respect to Z, U,W : the displacements at Z-section. The notations in this equation are explained in Fig.1. The rate of this equation gives the incremental strain ($\dot{E}$) expressed by Eq.(2).

$$\dot{E}=\dot{W}'+U'\dot{U}'-\dot{U}''X \qquad (2)$$

in which the dots mean the increment.

5) The incremental plastic strains ($\dot{E}pa$,$\dot{E}pb$) are expressed by Eq.(3).

$$\dot{E}pa=Ra(1-Z/Za)\dot{E}e \quad \text{at } X=d,\ Z=(0,Za)$$
$$\dot{E}pb=Rb(1-Z/Zb)\dot{E}e \quad \text{at } X=-d,\ Z=(0,Zb) \qquad (3)$$

in which Ra,Rb : the ratio of the incremental plastic strain to the incremental elastic strain, Za,Zb : the length of the plastic zone along the axis, $\dot{E}e$: the incremental elastic strain, d : the half distance between the concentrated sections. The distribution of the incremental strains and the notations are explained in Fig.2. The values of Ra,Rb are decided according to the hysteretic stress-strain relation at the fixed end. The stress-strain relation is expressed by the tri-linear model shown in Fig.3.

6) The shear deformation is neglected.

2.2 The equivalent two-flange section

Fig.4 shows the moment-axial force (M-N) interaction of the section of a steel member which is defined by the ultimate stress (Mu,Nu). The relation is generally expressed by the curved line as shown by the real line in the figure. However, the M-N relation of the two-flange section explained in the assumption 2) is given by the straight line as shown by the dashed line in Fig.4.

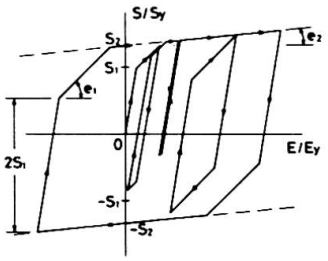

Fig.3 Stress-Strain Relation

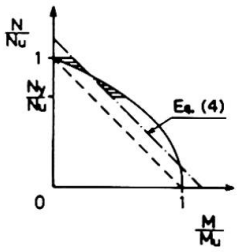

Fig.4 M-N Interaction

In this case the error is too large to analyze bracing members which are subjected to high tensile axial load. To exclude this error, in this study the concentrated areas (Aa,Ab) of the replaced equivalent two-flange section are given under the condition to minimize the sum of the difference between the two curves over the yield axial force (Ny) which is shown by the shaded area in Fig.4. Although the values of Aa,Ab should be changed according to the sectional shape of member, to simplify the calculation, Aa,Ab are given by the representative values shown in Eq.(4).

$$Aa=0.8*A, \quad Ab=0.2*A \qquad (4)$$

where Aa : the sectional area of the higher stress flange, Ab : the sectional area of the other flange, A : the sectional area of the original section.

2.3 The incremental elastic strain

The incremental strain ($\dot{E}$) of the model presented in this study is divided into the three components which are the incremental elastic strain ($\dot{E}e$) and the incremental plastic strains ($\dot{E}pa$,$\dot{E}pb$). The elastic strain component among them will be expressed by the end-deformations.

According to the assumption 4), the incremental elastic strain component can be expressed by Eq.(5).

$$\dot{E}e=\dot{W}e'+U'\dot{U}e'-\dot{U}e''X \qquad (5)$$

The suffix e means the elastic component. As the loads (Fx,Fz,Fr) work only at the free end of the model, the incremental elastic strain at the center of section ($\dot{E}oe$) is constant along the axis and it is given by Eq.(6).

$$\dot{E}oe=\dot{W}e'+U'\dot{U}e' \qquad (6)$$

The incremental curvature ($\dot{U}e''$) which is generated by the incremental elastic strain is the linear function of Z due to the assumption 3). From this condition and the boundary condition at the fixed end, the incremental deflection ($\dot{U}e$) caused only from elastic strain can be expressed by the incremental end-deformations ($\dot{D}xe$,$\dot{D}re$). The incremental end-displacement ($\dot{D}ze$) in Z-direction due to the elastic strain is derived from Eq.(6) and it is expressed by Eq.(7).

$$\dot{D}ze=\int(\dot{E}oe-U'\dot{U}e')dZ \qquad (7)$$

Substituting $\dot{W}e'$,$\dot{U}e'$ and $\dot{U}e''$ expressed by the incremental end-deformations into Eq.(5), we obtain the following equation.

$$\dot{E}e=[e][\dot{D}e] \qquad (8)$$

where $[\dot{D}e]=[\dot{D}xe/L\ \dot{D}ze/L\ \dot{D}re]'$, [ ]' means the transposed matrix.

2.4 The incremental plastic end-deformations

The incremental plastic strain is divided into the two components ($\dot{E}pa$,$\dot{E}pb$) whose distributions are shown in Fig.2. Using the assumption 4), the components can be expressed by Eqs.(9).

$$\dot{E}pa=\dot{E}opa-\dot{U}pa''X \quad \text{at } X=d,\ Z=(0,Za)$$
$$\dot{E}pb=\dot{E}opb-\dot{U}pb''X \quad \text{at } X=-d,\ Z=(0,Zb) \tag{9}$$

$\dot{E}opa$,$\dot{E}opb$ are the incremental plastic strain at the center of the section (X=0). $\dot{U}pa$,$\dot{U}pb$ are the incremental plastic deflection caused from $\dot{E}pa$,$\dot{E}pb$ respectively. $\dot{E}pa$,$\dot{E}pb$ are defined so as to satisfy Eqs.(10) respectively.

$$\dot{E}opa=\dot{E}pa/2, \quad \dot{E}opb=\dot{E}pb/2 \tag{10}$$

Substituting Eqs.(8),(9) and (10) into Eq.(3), the following relations are derived.

$$Ra(1-Z/Za)[e][\dot{D}e]=-2d*\dot{U}pa'', \quad Rb(1-Z/Zb)[e][\dot{D}e]=2d*\dot{U}pb'' \tag{11}$$

The functions $\dot{U}pa$,$\dot{U}pb$ in Eq.(11) are obtained by the use of the boundary conditions at the fixed end.

The incremental plastic end-deformations ($\dot{D}xp$,$\dot{D}zp$,$\dot{D}rp$) caused from the incremental plastic strain components ($\dot{E}pa$,$\dot{E}pb$) are given by Eqs.(12) and (13).

$$\dot{D}xp=\dot{U}pa+\dot{U}pb, \quad \dot{D}rp=\dot{U}pa'+\dot{U}pb' \quad \text{at } Z=L \tag{12}$$

and

$$\dot{D}zp=\int(\dot{E}opa+\dot{E}opb-U'(\dot{U}pa'+\dot{U}pb'))dZ \tag{13}$$

In the equations $\dot{D}xp$,$\dot{D}zp$ are the incremental plastic end-displacements in X-direction and in Z-direction respectively. $\dot{D}rp$ is the incremental plastic end-rotation. $\dot{E}opa$,$\dot{E}opb$ in Eq.(13) can be expressed by $\dot{U}pa$,$\dot{U}pb$ from Eqs.(9) and (10). Substituting $\dot{U}pa$,$\dot{U}pb$ into Eqs.(12) and (13), we get Eq.(14).

$$[\dot{D}p]=[T][\dot{D}e] \tag{14}$$

where $[\dot{D}p]=[\dot{D}xp/L\ \dot{D}zp/L\ \dot{D}rp]'$.

The integrations in the matrix [T] are easily executed and they are expressed in the closed form function of the end-deformations $[\dot{D}e]$,$[\dot{D}p]$ because the deformation included in the integration can be expressed by Eq.(15)

$$U'=\Sigma(\dot{U}e'+\dot{U}pa'+\dot{U}pb') \tag{15}$$

where Σ means the summation of the increments.

2.5 The rate equation

The relation between the end-loads and the end-deformations of a steel member will be derived in this paragraph.

The incremental virtual work equation of the model, shown in Fig.1 and explained in the assumption 1), is given by Eq.(16).

$$[F]'[\dot{D}]=\int\int S.\dot{E}.dZdA/(PyL) \tag{16}$$

in which, $[F]=[Fx/Py\ Fz/Py\ Fr/(Py.L)]'$, $[D]=[Dx/L\ Dz/L\ Dr]'$, Py : the yield axial force, S : the normal stress and $\int dZ$,$\int dA$: the integration along Z-axis and over the sectional area respectively. The notations in Eq.(16) are explained in Fig.1.

The incremental strain $\dot{E}$ in Eq.(16) is the sum of the elastic component and the plastic components and it is shown by Eq.(17).

$$\dot{E}=\dot{E}e+\dot{E}pa+\dot{E}pb \tag{17}$$

The incremental strains in the right side of Eq.(17) can be expressed by the function of $[\dot{D}e]$ by substituting Eqs.(3) and (8) into Eq.(17) and we find

$$\dot{E}=(1+Ra(1-Z/Za))[e][\dot{D}e] \quad \text{at } X=d,\ Z=(0,Za)$$
$$\dot{E}=(1+Rb(1-Z/Zb))[e][\dot{D}e] \quad \text{at } X=-d,\ Z=(0,Zb) \tag{18}$$

Since $[\dot{D}]=[\dot{D}e]+[\dot{D}p]$, $[\dot{D}e]$ can be expressed by $[\dot{D}]$.

$$[\dot{D}e]=inv[To][\dot{D}] \tag{19}$$

in which [To]=[T]+[1] and "inv" means the inverse matrix.
The equilibrium equation is derived by substituting Eqs.(18) and (19) into Eq.(16).

$$[F]=inv[To]'\int(\int S(1+Ra(1-Z/Za))[e]'dA+\int S(1+Rb(1-Z/Zb))[e]'dA)dZ/PyL \tag{20}$$

The rate equation of Eq.(20) becomes

$$[To]'[\dot{F}]=[k][\dot{D}e] \tag{21}$$

Substituting Eq.(19) in Eq.(21) we finally obtain the relation between $[\dot{F}]$ and $[\dot{D}]$.

$$[\dot{F}]=[K][\dot{D}] \tag{22}$$

in which [K]=inv[To]'[k]inv[To]. [K] is the tangent stiffness matrix of the structural model. It is defined by the tangent modulus of the stress-strain relation and the residual deformations. In the presented stiffness matrix in Eq.(22) the influence of the residual deformations is expressed in the closed form function in which only the sum of the incremental end-deformations $[\dot{D}e],[\dot{D}p]$ and the plastic zone length (Za,Zb) are included. This expression of the residual plastic deformation in the stiffness matrix makes the presented method very simple.

2.6 The plastic zone length

Since the loads of the model works only at the free end, it is reasonable to assume that the incremental normal stress distributes linearly along the axis of the member. But the elastic limit stress may not distribute linearly along the axis according to the hysteretic plastic deformation. To simplify the calculation of Za,Zb, the critical stress of elastic range is also assumed to distribute linearly. Under this condition the plastic zone length is easily obtained as the intersection point of the two linear functions of Z.

2.7 Application to steel member and steel frame

If every steel member of building frames is divided into the two parts along the axis, each part can be considered as the cantilever member whose loading condition is the same as shown in Fig.1 and the load-deformation relation is given by Eq.(22). From this reason the relationships between the end-loads and the end-deformations of every steel member can be derived by coupling the two presented equations, shown by Eq.(22), under the continuation conditions at the center along the axis of the member. The derived load-deformation relation is easily applied to the analysis of steel frames.

3. NUMERICAL ANALYSIS

To show the usefulness of the presented analysis method, the numerical analysis of plane steel frames under seismic load has been carried out. The analyzed steel frames, named Frame-1 and Frame-2, are 10-story 3-bay braced frames shown in Fig.5. Frame-1 is designed based on the Japanese Aseismic Design Code and the horizontal strength and the stiffness of every story are perfectly agree with the required criteria of the code. To simulate the collapse behavior, Frame-2 is designed under the half of the seismic load of Frame-1. The ground motion is the N-S component of the well-known El Centro 1940 record amplified by three times. The calculation of the seismic response has been carried out by the use of the linear-acceleration method under the condition that the errors of the energy balance equation [6] does not exceed 0.5 percent of the input energy.

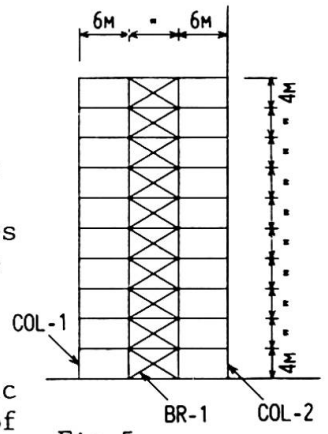

Fig.5 Calculated Frame

Numerical results are shown in Figs.6-9. From these figures we can say the inelastic hysteretic behavior and the collapse behavior of the frames are analyzed fairly well. It is also shown that the restoring force characteristics of the columns, which effect strongly on the response of the frames, are remarkably complicated and different mutually and the deformation of the frames tends to be concentrated only in one story. These results emphasize that in the analysis of

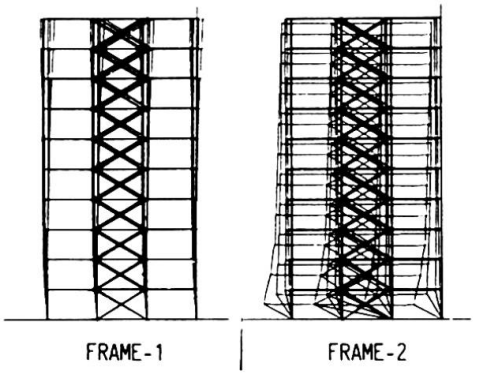

Fig.6 Deflected Shape (in Real Proportional Scale)

steel frames the detailed behavior of all members should be analyzed.

4. CONCLUSIONS

i) The proposed analysis method is simple and does not require so much calculation but it can simulate the hysteretic inelastic behavior of steel members under intense loads relatively accurately. Since the presented method is applicable to columns, beams and braces in the same manner, it is useful and suitable for the detailed structural analysis of building frames without a large amount of calculation.

ii) The collapse of building frames is caused from the failure of a few members whose restoring force characteristics are very complicated. Accordingly it is necessary for the reliable structural analysis of tall buildings, which are composed of many members, to analyze the detailed behavior of all members accurately.

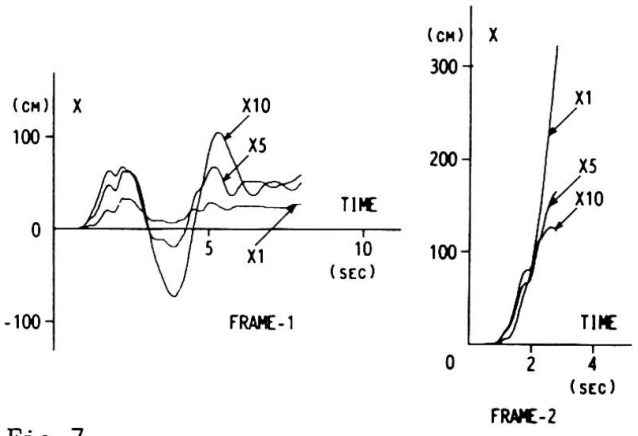

Fig.7
Time Histories of Response Displacement

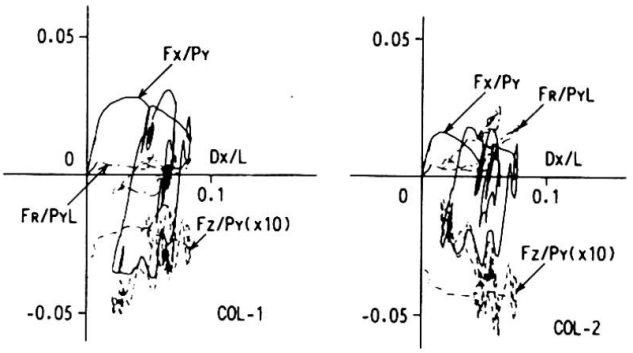

Fig.8
Hysteretic Behavior of Columns

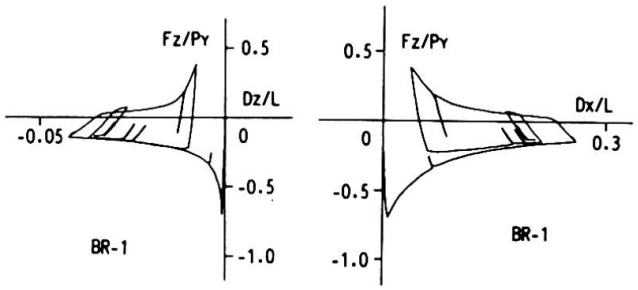

Fig.9
Hysteretic Behavior of Brace

REFERENCES

1. NONAKA,T., "An Elastic-Plastic Analysis of a Bar under Repeated Axial Loading," Int. J. Solids Structures, Vol.9, 1973.
2. IGARASHI,S.,INOUE,K.,KIBAYASHI,M. and ASANO,M., "Hysteretic Characteristics of Steel Braced Frames, Part 1," Trans. of the Architectural Institute of Japan, Vol.196, June,1972.
3. FUJIWARA,T., "Earthquake Response of Framed Structures Having Aseismic Elements, Part I," Trans. of the Architectural Institute of Japan, NO.285, Nov.,1979.
4. SHIBATA,M. and WAKABAYASHI,M., "Elastic-Plastic Analysis of Steel Braced Frame Subjected to Repeated Horizontal Load," Trans. of the Architectural Institute of Japan, No.325, March,1983.
5. MAHIN,S.A. and IKEDA,K., "A Refined Physical Theory Model for Predicting the Seismic Behavior of Braced Steel Frames," Univ. of California Berkeley, EERC 84/12, July,1984.
6. TANABASHI,R., NAKAMURA,T. and ISHIDA,S.,"Gravity Effect on the Catastrophic Dynamic Response of Strain-Hardening Multi-Story Frames," Proc. of the 5-th World Conference of Earthquake Engineering, June,1973.
7. SAISHO,M., "Analysis of Braces by Cantilever Member Elements with the Equivalent Two-Flange Section," Annual Meeting of the Architectural Institute of Japan, August,1986.

Strength, Stiffness and Nonlinear Behaviour of Simple Tubular Joints

Résistance, rigidité et comportement non linéaire d'assemblages tubulaires simples

Festigkeit, Steifigkeit und nicht-lineares Verhalten von einfachen Knotenpunktsverbindungen aus Rundhohlprofilen

Pentti MÄKELÄINEN
Assoc. Prof.
Helsinki Univ. of Techn.
Espoo, Finland

Ram PUTHLI
Dr.Eng.
TNO-IBBC
Rijswijk, The Netherlands

Frans BIJLAARD
Civil Engineer
TNO-IBBC
Rijswijk, The Netherlands

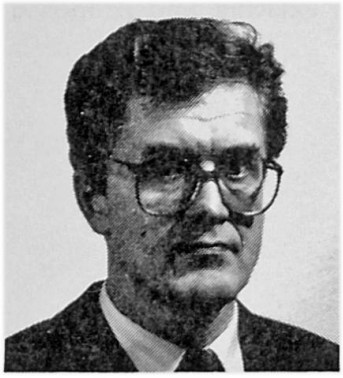

Pentti Mäkeläinen, born 1944, obtained his engineering degree and his doctoral degree at Helsinki University of Technology. Since 1969 he has been working in the Department of Civil Engineering as a research assistant, a lecturer, an associate professor and an acting professor of Structural Mechanics and of Steel Structures.

Ram Puthli, born 1944, graduated in Civil Engineering from I.I.T. Kharagpur, India in 1964. He obtained his M.Sc (Structures) from Manchester University and Ph.D. from Surrey University. He has ten years experience in Industry and twelve years in Research. He has been involved in research at TNO-IBBC since 1979.

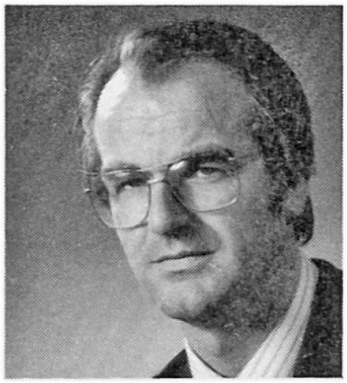

Frans Bijlaard, born 1947, graduated as Civil Engineer at the Technical University Delft. For the last ten years he has been concerned with research on stability and connections in steel structures. At present he is Head of the Department of Steel Structures of the TNO Institute for Building Materials and Structures.

SUMMARY

The present work describes a wide investigation on joint behaviour. Semi-analytical formulae are established for initial stiffness, strength under single and combined loading, and the secant stiffness at any load up to collapse. This information is sufficient to plot the complete non-linear behaviour until collapse and to determine the stiffness at working loads. All this work has been checked against experimental data from a large data bank. The work on simple multibraced joints is incomplete because of the absence of experimental data for these joints.

RÉSUMÉ

Cette étude présente une vaste recherche sur le comportement d'assemblages. Des formules semi-analytiques donnant la rigidité initiale, la résistance pour des charges simples et combineés ainsi que la rigidité sécante, ont été établiés pour des charges allant jusqu'à la limite de rupture. Cette information suffit pour décrire complètement le comportement non linéaire jusqu'à la rupture ainsi qu'à déterminer la rigidité aux charges d'exploitation. Tous les résultats de cette recherche ont été vérifiés en les comparant à des données expérimentales. L'étude faite sur les assemblages simples à branches multiples est incomplète puisqu'il manque des données expérimentales.

ZUSAMMENFASSUNG

Die vorliegende Forschungsarbeit beschreibt eine breite Untersuchung des Verhaltens von T und DT Knotenpunktsverbindungen. Halb-analytische Formeln werden gegeben für Anfangssteifigkeit, Festigkeit unter einfacher und mehrfacher Belastung und für die Sekantensteifigkeit bei jeder Belastung bis zum Erreichen der Traglast. Diese Daten sind ausreichend, um das ganze nicht-lineare Verhalten bis zum Erreichen der Traglast darzustellen und um die Steifigkeit bei der vorhandenen Belastung zu bestimmen. Die gesamte Forschungsarbeit wurde verglichen mit experimentellen Daten aus einer grossen Datenbank. Die Arbeit an mehrfachen Knotenpunktsverbindungen ist nicht komplett weil experimentelle Daten fehlen.

1. INTRODUCTION

Tubular lattice girders and frames are popular in various building and offshore structures, so that tubular joints of various kinds are very common. The structural behaviour of such joints is complex, with each type of joint, its parametric variation of geometry and type of loading having considerable influence on the strength and stiffness characteristics.

This paper is restricted to T and DT (Double Tee) joints with loaded braces under single and combined (proportional) loading and as a special case, multibraced joints with loaded and unloaded braces (Fig. 1). Simple formulae have been established for the joint stiffness, strength and non-linear behaviour of these joints. Semi-analytical models are used as a basis, and a large experimental data bank used to assess the values from existing and proposed formulae.

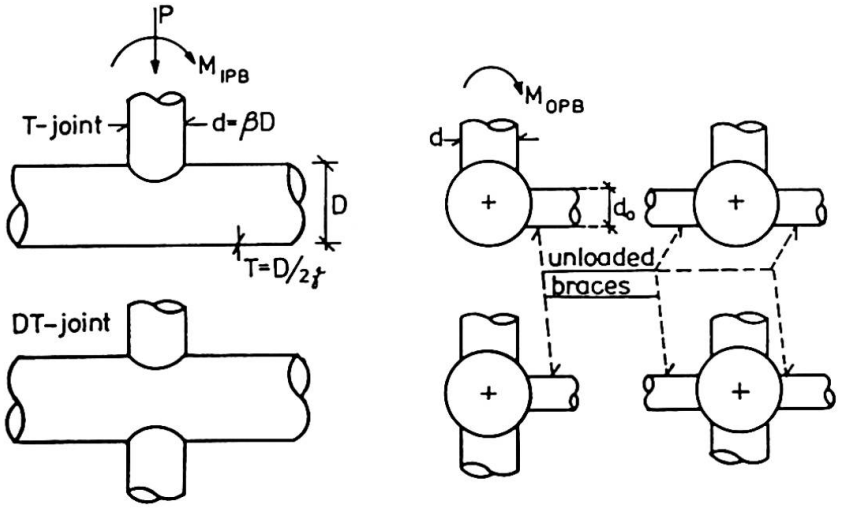

Fig. 1 Joint types investigated

2. ANALYTICAL MODELS FOR INITIAL JOINT STIFFNESS

2.1 T and DT joints

Empirical formulae are available for the initial joint stiffness (or flexibility) of T and Y joints only,[3,4,5], which gives stiffness values higher than those observed experimentally. Experimental studies using epoxy resin (Araldite) models, gives consistently higher stiffness values than those with steel models for all cases (see Figs. 2,3,4). This may be due to different material properties and effect of weld intersection.

The real complex behaviour of T and DT joints under axial and OPB moment loading of the brace can be approximated by using a simplified model where the three dimensional behaviour of the joint is represented by assuming a two dimensional ring (Fig. 2). The following derivation is made for the initial axial stiffness K_o :

$$K_o = P/\delta_o = \frac{(B_e/D)}{\gamma^3 f_o(\beta)} ED = k_o ED \tag{1}$$

where $f_o(\beta)$ is a complicated function of β and $\alpha = arcsin\beta$. This function $f_o(\beta)$ can be closely approximated by the function $(1-\beta)^s$ where the exponent "s" has an average value of 1.13. By assuming a power law dependence upon γ for B_e/D and then fitting all the

available experimental data to equation (1), a formula (2) presented in Fig.2 can be found for K_o of T joints. Similarly, this procedure gives formula (3) shown in Fig. 3 for the initial OPB stiffness of T joints.

Fig. 2 gives a plot of all the initial axial stiffness data of T joints versus β. Formula (2) is expressed with lines of constant γ values of 8, 15 and 24, showing reasonable agreement with the data points. Test values on plastic (epoxy) tubes [4] are also shown in Fig. 2.

Fig. 3 gives a plot of all the initial OPB stiffness data of T joints and a formula (3) based on a similar procedure, along with the data points from tests on plastic tubes.

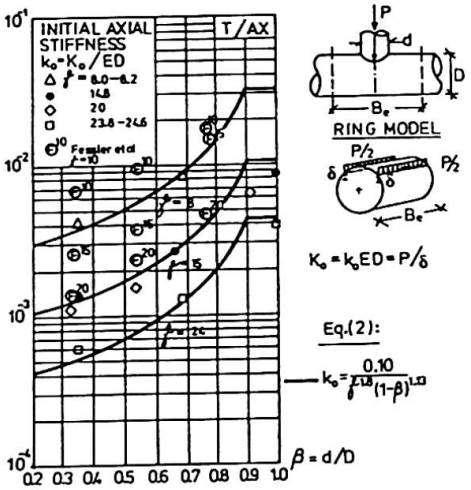

Fig. 2 Initial axial stiffness of T joints vs. β

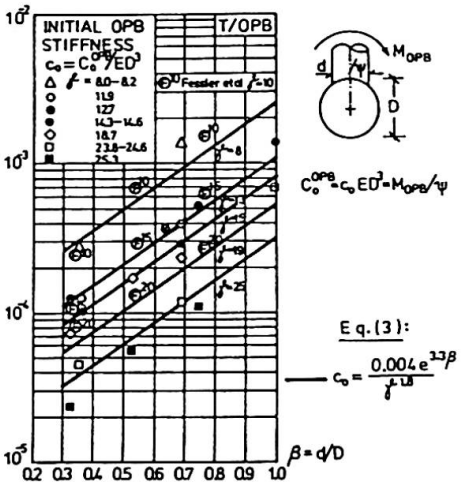

Fig. 3 Initial OPB stiffness of T joints vs. β

The analogy of a beam on elastic foundations (BEF) is applied for the initial IPB stiffness of T joints by assuming the section of the chord between brace saddle points as a beam over the entire chord length, supported by the remaining sector as a BEF along at the two longitudinal edges of the beam. On the basis of the expressions derived for the foundation stiffness (k_f) and bending stiffness of the beam (EI_b), a formula (4) shown in Fig. 4 is developed for the IPB stiffness of T joints. Fig. 4 shows all the relevant experimental data for the IPB stiffness of T joints (with formula (4)) plotted as lines of constant γ (10, 15, 25). Data points are also shown from the tests on plastic tubes [4]. Similar comparisons as above with the available experimental data and formulae based on the ring model and the analogy of a beam on elastic foundations are also developed for approximating the initial axial, OPB and IPB stiffness of DT joints [1].

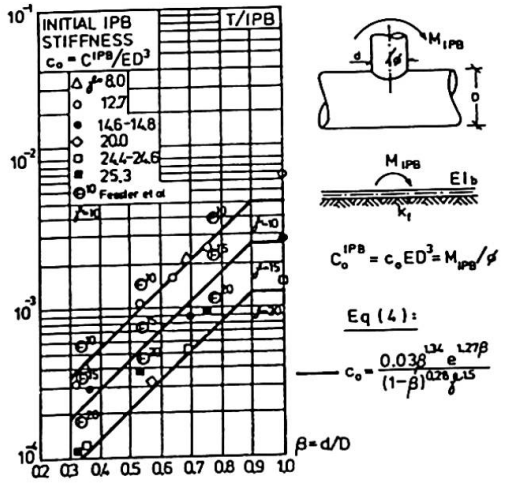

Fig.4 Initial IPB stiffness vs. β

2.2 Simple multibraced joints with unloaded braces

Formulae for the initial axial and OPB stiffness of simple multi-braced DT and T joints with unloaded braces in a perpendicular plane to loaded braces can be derived by applying the ring model where a rigid cap between the brace saddle points is assumed. Because of the enormous complexity of the cases with only one unloaded brace in the joint, only symmetrical cases of DT and T joints with two unloaded braces have been considered at present. Joint stiffness

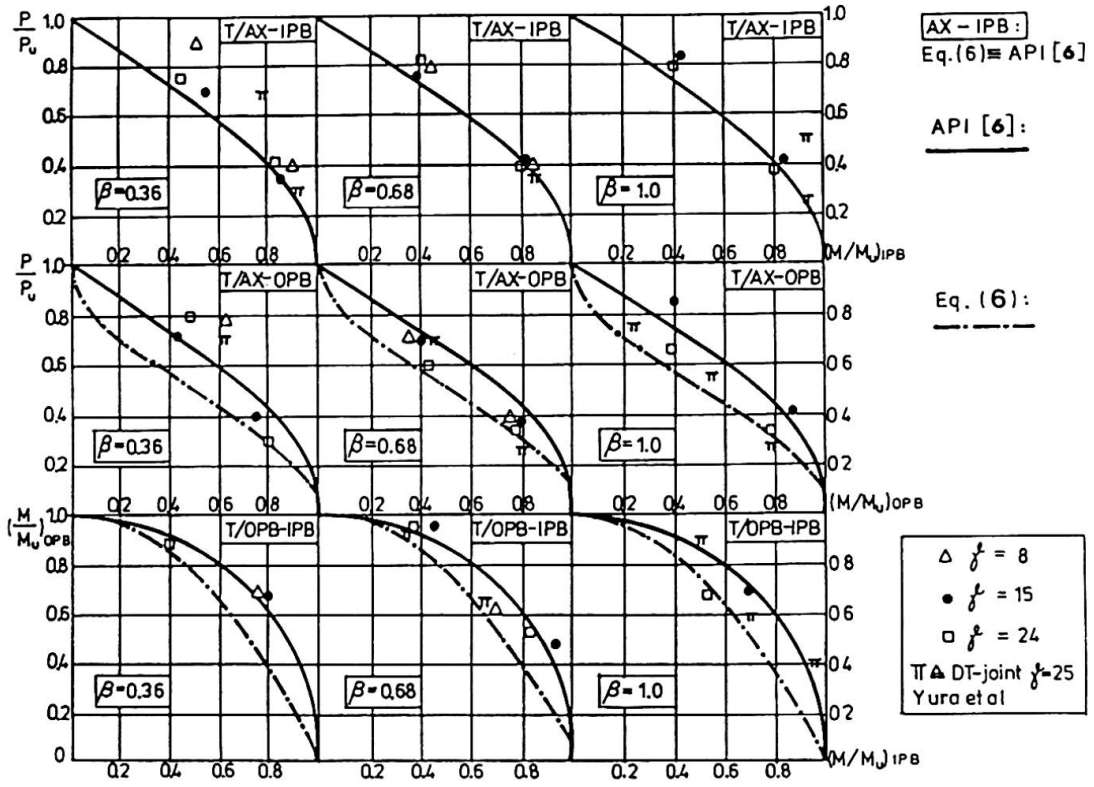

Fig. 5 Results of 2D interaction tests (AX-IPB,AX-OPB,IPB-OPB) for $\beta = 0.36, 0.68, 1.0$

equations derived on the basis of the above model cannot be further developed and calibrated because of the lack of experimental data. Experimental testing of these joints planned to be carried out in the near future will provide some reliable data points for finalizing the model.

3. JOINT STRENGTH MODELS UNDER SINGLE BRACE LOADS

A number of basic failure modes or their combinations are identified for DT and T joints under single brace loads [2] depending upon the joint parameters and loading conditions. Semi-analytical models such as ring models with plastic hinges [2,9] and the punching shear model [2] have been used. The present work extends this theory for axial load and OPB moment. For IPB moment a BEF analogy has also been used. Because of the complexity of the derived formula and the scatter (or lack) of experimental data, the calibration of the formulae have not yet been performed. This work has taken lower precedence because of recent international agreement [7] on comprehensive, simple design rules. However, an insight into the failure modes has been obtained.

The ultimate strength of simple multi-braced joints with unloaded braces is also studied on the same lines as above. In this case, however, no experimental data is available yet for calibrating the models.

4. JOINT STRENGTH UNDER COMBINED BRACE LOADS

In service the joints, especially in three dimensional tubular structures, are subjected to the combined action of axial and bending moment (IPB and OPB) loads in the brace. Only T and DT joints are considered. Ultimate brace loads due to interaction effects are further complicated due to the dependence upon the load vector and whether the loading is incremented

proportionally or non-proportionally. Therefore, only empirical approaches have been used. Such a formula is [8]:

$$\frac{P}{P_u} + \left(\frac{M}{M_u}\right)^{2.1}_{IPB} + \left(\frac{M}{M_u}\right)^{1.2}_{OPB} = 1 \tag{5}$$

The above formula does not fit the experimental results [10]. A semi-analytical interaction equation is suggested for T and DT joints, based upon a modification to the theoretical plastic strength of tubular section:

$$\frac{P}{P_u} + \frac{2}{\pi} arcsin\sqrt{\left(\frac{M}{M_u}\right)^2_{IPB} + \left(\frac{M}{M_u}\right)_{OPB}} = 1 \tag{6}$$

The API rules [6] use the unmodified formula. Both the API rules [6] and equation (6) take the IPB-OPB coupling effect into account, which equation (5) does not.

An inspection of the 2 D interaction plots of all the available experimental data in Fig. 5 shows that the collapse mecanisms are different, with the API rules [6] unable to give safe lower bounds to the interaction data. A check is also carried out against 3 D interaction ($P - M_{IPB} - M_{OPB}$) by substituting test results [10] into equation (6). The results confirm that the generated yield surface is a reasonable lower bound also for 3D behaviour. This is also valid for 3D interaction tests on DT joints [11].

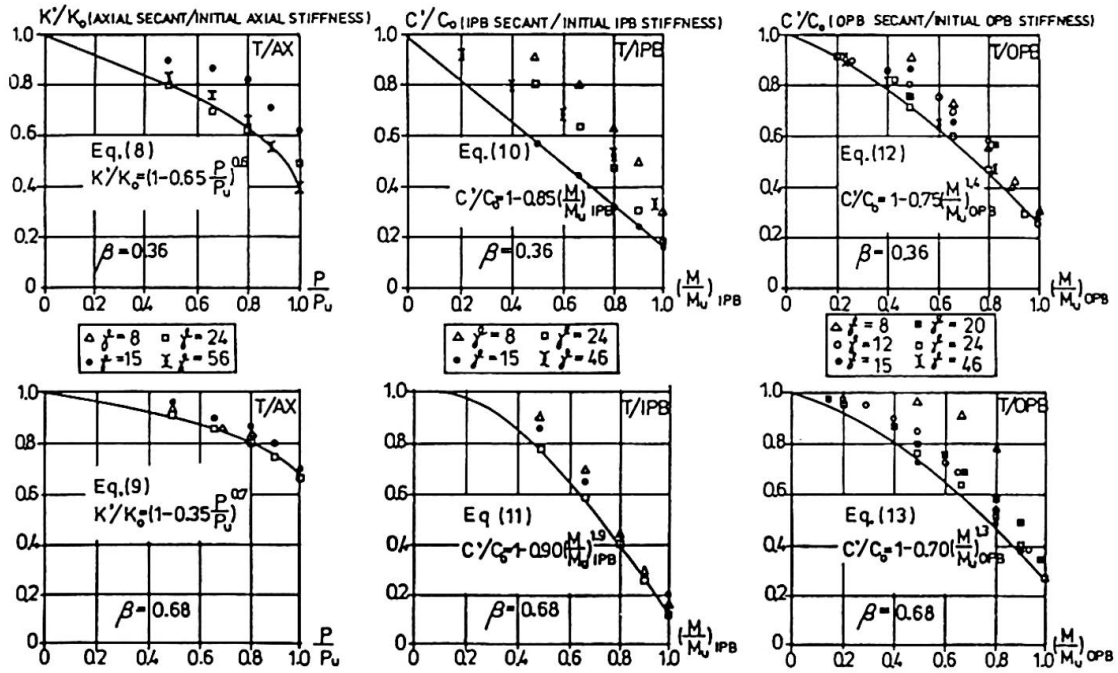

Fig. 6 Normalized axial, IPB and OPB secant stiffnesses of T joints for $\beta = 0.36$ and 0.68

5. NON-LINEAR JOINT BEHAVIOUR UNDER SINGLE BRACE LOADING

Normalized secant stiffness values at various normalized load levels (as a percentage of ultimate load) have been recorded from the experimentally obtained non-linear load-deflection plots in the data bank, as shown for T joints in Fig. 6. DT joints have also been treated similarly [1]. Lower bound equations such as shown in Fig. 6 have been deduced, based upon the lowest experimentally obtained secant stiffnesses. Once the initial stiffness (K_o, C_o) and the ultimate load (P_u, M_u) are known or calculated from formulae, the secant stiffness at

various load levels can be determined from these equations to retrace the complete non-linear behaviour. If necessary, the tangent stiffness can also be determined from the equation or the non-linear plot using two close load levels. In this way, correct joint stiffnesses may be derived for any design criteria under working load levels.

6. CONCLUSIONS

Initial stiffness and strength formulae have been established or confirmed for T and DT joints under single brace loading. This will be done for simple multibraced joints when planned experimental work is completed. A lower bound interaction formula is also established for joint strength under combined loading for T and DT joints, which satisfies all experimental data. Finally, lower bound stiffness formulae for tracing the non-linear behaviour of T and DT joints up to ultimate load have been established. This can be useful in calculating the tangent or secant stiffness at any (working) load level in accordance with design criteria.

REFERENCES

1. MÄKELÄINEN, P.K., PUTHLI, R.S. and BIJLAARD, F.S.K., Strength, Stiffness and Non-Linear Behaviour of Simple (Multi Braced) Welded Tubular Joints. TNO-IBBC Report No. BI-87-72, Delft, The Netherlands, June 1987.

2. WARDENIER, J., Hollow Section Joints. Delft University Press/1982.

3. Det norske Veritas (DnV): Rules for the Design, Construction and Inspection of Offshore Structures. Appendix C: Steel Structures. Oslo 1977.

4. FESSLER, H., et. al., Parametric Equations for the Flexibility Matrices of Single Brace Tubular Joints in Offshore Structures. Proc. Instn. Civ. Engrs., Part 2, Vol. 81, Dec. 1986.

5. EFTHYMIOU, M., Local Rotational Stiffness of Unstiffened Tubular Joints. Koninklijke/Shell Exploratie en Produktion Laboratorium, Rijswijk, Rep. No. RKER. 85.199 1985.

6. American Petroleum Institute (API): Recommended Practice for Planning, Designing and Constructing Fixed Offshore Platforms. RP2A, 15th Edition, Oct. 1984.

7. International Institute of Welding (IIW): Design Recommendations for Hollow Section Joints. IIW-XV-E, Doc. XV-491-81/XIII-1003-81 (revised version to be published in 1988).

8. Underwater Engineering Group (UEG) Offshore Research Document: Design of Tubular Joints for Offshore Structures. Vol. 1,2 and 3. UEG/CIRIA 1985.

9. TOGO, T., Experimental Study on Mechanical Behaviour of Tubular Joints. Doctorial Dissertation (in Japanese). Osaka University, Osaka 1967.

10. STOL, H.G.A., PUTHLI, R.S. and BIJLAARD, F.S.K., Static Strength and Stiffness of As-Welded Tubular T-Joints under Proportionally Applied Combined Static Loading. TNO-IBBC Report No. B-84-561, Parts I, II and III. Delft, The Netherlands. April 1985.

11. YURA, J.A. and SWENSSON, K.D., Strength of Double-Tee Tubular Joints: Interaction Effects. Phase 3 Final Report, Vol. 3 of 3, The University of Texas at Austin, July 1986.

Stiffener Eccentricity in Theory of Orthotropic Plates

Excentricité des raidisseurs dans la théorie des plaques orthotropes

Steifenexzentrizität in der Theorie orthotroper Platten

Ivan BALÁŽ
Dr.Eng.
Slovak Techn. Univ.
Bratislava, ČSSR

Ivan Baláž, born 1948, received his Civil engineering degree at the STU in 1973. For four years he was involved in stability problems of orthotropic plates at the Slovak Academy of Sciences, Bratislava. Since 1978 he has been working at Faculty of Civil Engineering, STU Bratislava as assistant lecturer.

SUMMARY
The paper is concerned with the effect of stiffener eccentricity on the critical stress and on the elastic postcritical behaviour of orthotropic plates in compression. The non-linear theory takes account of initial geometrical imperfections and of large displacements. The problem has been studied on four large scale steel models. The first results have shown that effect of stiffener eccentricity is practically negligible.

RÉSUMÉ
L'article traite l'influence de l'excentricité des raidisseurs sur la contrainte critique et sur le mouvement élastique postcritique des plaques orthotropes comprimées. La théorie non-linéaire prend en considération les flèches initiales et les grandes déformations. On étudie ce problème sur quatre modèles d'acier. Les premiers résultats montrent que l'influence de l'excentricité des raidisseurs est pratiquement négligeable.

ZUSAMMENFASSUNG
Der Aufsatz beschäftigt sich mit dem Effekt der Steifenexzentrizität auf die kritische Spannung und auf das elastische überkritische Verhalten der druckbeanspruchten orthotropen Platten. Die nichtlineare Theorie berücksichtigt anfängliche Verformung und größere Durchbiegungen. Das Problem wurde an vier großen Stahlmodellen untersucht. Die ersten Ergebnisse zeigten, daß der Einfluß der Steifenexzentrizität praktisch vernachlässigbar ist.

1. INTRODUCTION

During the last seventeen years intensive research programmes, both theoretical and experimental, have been undertaken in the field of orthotropic plates in compression as a result of the four collapses of long span box girder bridges that occured between 1969 and 1971. Extensive studies have influenced the design codes, and design rules based on the postcritical behaviour of plated structures have been established.
Two most widely adopted approaches are usually considered in the study of the stiffened plate behaviour: /i/ the strut approach and /ii/ the orthotropic plate approach. The latter is analysed in the present paper.
In this approach, the stiffened plate is treated as an equivalent orthotropic plate and the elastic large deflection theory is used.

MAQUOI and MASSONNET /1971/ developed a design method that takes account of postcritical strength increases produced by membrane stresses. The main assumptions of this analysis are as follows:
- the rigidities of the stiffeners can be smeared in order to obtain a substitute plate that is then analysed by a non-linear large displacement theory;
- the postbuckling shape of the plate is represented by only its first term of the double FOURIER series expansion;
- collapse is reached when the mean longitudinal membrane stress along the unloaded edges of the orthotropic panel reaches yield stress f_y. The flexural stresses are neglected;
- allowance for plate buckling between the stiffeners is made by using an effective width approach.

Starting from the Liege method [9], an attempt [1] has been undertaken to improve the above-mentioned approach:
- it has been able to take account of several terms of a FOURIER expansion and
- to prepare design formulae which simplify considerably the mathematical procedure and present therefore the ultimate strength theory of stiffened plates in a form suitable for practical use in designing bureaux;
- simply supported orthotropic plate in compression with more complex in-plane boundary conditions has been solved in [1] and solution comprises case of isotropic plate too and/or transversely loaded plates;
- relating collapse to the maximum membrane stress - rather than the mean membrane stress along the unloaded edges - has enabled to avoid any plastic redistribution of the membrane stresses.

The theoretical and the numerical results of the thesis [1] can be found also in the chapter 7 of the book [5]. Results of a parametric study were published also in [3].

In addition, it has been analysed in the paper [2]:
- the combined effect of the membrane stresses and the flexural stresses on the limit state by using several various collapse criteria;
- the shear lag phenomenon determined according to the new edition of the code ČSN 73 6205 "Design of Steel Bridge Structures";
- the comparisons of the theoretically obtained values and the experimental data of the ultimate load tests on 34 steel girders and 34 orthotropic plates in compression.

The aim of the present paper is to demonstrate a solution of the following system of two simultaneous differential equations describing of slender orthotropic plates with unsymmetrically arranged stiffeners and with an initial deflection

$$\bar{D}_x\frac{\partial^4 w}{\partial x^4}+2\bar{H}\frac{\partial^4 w}{\partial x^2\partial y^2}+\bar{D}_y\frac{\partial^4 w}{\partial y^4}+\frac{\nu}{1-\bar{\nu}^2}\left(e_x\frac{S}{S_y}\frac{\partial^4\Phi}{\partial x^4}+e_y\frac{S}{S_x}\frac{\partial^4\Phi}{\partial y^4}\right)-\frac{e_x+e_y}{1-\bar{\nu}^2}\frac{\partial^4\Phi}{\partial x^2\partial y^2}-\frac{\partial^2\Phi}{\partial x^2}\frac{\partial^2(w_0+w)}{\partial y^2}- \quad (X=0)$$

$$-\frac{\partial^2\Phi}{\partial y^2}\frac{\partial^2(w_0+w)}{\partial x^2}+2\frac{\partial^2\Phi}{\partial x\partial y}\frac{\partial^2(w_0+w)}{\partial x\partial y}-q=0 \qquad (1a)$$

$$\frac{1}{S_y}\frac{\partial^4\Phi}{\partial x^4}+\frac{2}{\bar{S}}\frac{\partial^4\Phi}{\partial x^2\partial y^2}+\frac{1}{S_x}\frac{\partial^4\Phi}{\partial y^4}=(1-\bar{\nu}^2)\left\{\left|\frac{\partial^2(w_0+w)}{\partial x\partial y}\right|^2-\frac{\partial^2(w_0+w)}{\partial x^2}\frac{\partial^2(w_0+w)}{\partial y^2}-\right. \qquad (1b)$$

$$\left.-\left[\left(\frac{\partial^2 w_0}{\partial x\partial y}\right)^2-\frac{\partial^2 w_0}{\partial x^2}\frac{\partial^2 w_0}{\partial y^2}\right]\right\}+\nu S\left(\frac{e_x}{S_y}\frac{\partial^4 w}{\partial x^4}+\frac{e_y}{S_x}\frac{\partial^4 w}{\partial y^4}\right)-(e_x+e_y)\frac{\partial^4 w}{\partial x^2\partial y^2}$$

Equations (1) generalize the well-known equations of FÖPPL-von KÁRMAN-MARGUERRE and HUBER´s equation. Earlier solutions [1,2,3,5,9] neglected the terms of the equations (1) that contain excentrities e_x, e_y.

2. SOLUTION TO THE SYSTEM OF EQUATIONS

2.1 General

The system (1) is going to be solved by P.F. Papkovich´s method, which means that the compatibility equation (1b) will be solved exactly while the approximative method of B.G. GALERKIN will be employed in the solution to the equilibrium equation (1a).

2.2 Solution to the Compatibility Equation

The functions of the initial and additional deflections are supposed to have the form of a series in which all terms fulfil boundary conditions

$$\bar{w}_0=\sum_m\sum_n \bar{w}_{0mn}\sin m\pi\xi\sin n\pi\eta\,, \qquad \xi=\frac{x}{a},\ \eta=\frac{y}{b},\ \bar{w}=\frac{w}{t},\ \bar{w}_0=\frac{w_0}{t} \qquad (2a)$$

$$\bar{w}=\sum_m\sum_n \bar{w}_{mn}\sin m\pi\xi\sin n\pi\eta \qquad (2b)$$

The stress function is written as follows

$$\Phi^*=\Phi_0^*+\Phi_p^*\,, \qquad \Phi^*=\frac{\Phi}{S_y(1-\bar{\nu}^2)t^2} \qquad (3)$$

Φ_0^* being the general solution and Φ_p^* a particular integral of the compatibility equation.

After solution of the homogeneous compatibility equation we obtain

$$\Phi_0^*=\Phi_{00}^*+\Phi_{0i}^*+\Phi_{0j}^*=-\frac{\lambda^2}{2}(\bar{N}_x^*\eta^2+\bar{N}_y^*\xi^2\alpha^2)+\sum_i R_i^*(\eta)\cos i\pi\xi+\sum_j S_j^*(\xi)\cos j\pi\eta \qquad (4)$$

where
$$R_i^*(\eta)=A_i^*\cosh i\beta\eta+B_i^*\sinh i\beta\eta+C_i^*\cosh i\delta\eta+D_i^*\sinh i\delta\eta$$
$$S_j^*(\xi)=E_j^*\cosh j\gamma\xi+F_j^*\sinh j\gamma\xi+G_j^*\cosh j\varepsilon\xi+H_j^*\sinh j\varepsilon\xi \qquad (5)$$

The constants A_i^*, B_i^*, C_i^*, D_i^*, E_j^*, F_j^*, G_j^*, H_j^* are determined from the in-plane boundary conditions. In the case of boundaries being regarded as inflexible in the plate plane $A_i^*=B_i^*=C_i^*=D_i^*=0$ (boundaries parallel to axis X) and/or $E_j^*=F_j^*=G_j^*=H_j^*=0$ (boundaries parallel to axis Y).

The notation, which is not defined in the present paper, can be found in [1,2,5].

The particular integral, with regard (2), can be written in the following way:

$$\Phi_p^* = \Phi_{pw}^* + \Phi_{pe}^* = \tag{6}$$

$$= \frac{\alpha^2}{4} \sum_m \sum_n \sum_r \sum_s (\bar{w}_{mn}\bar{w}_{rs} + \bar{w}_{mn}\bar{w}_{0rs} + \bar{w}_{rs}\bar{w}_{0mn}) \times$$

$$\times \sum_{i=1}^{2} \sum_{j=1}^{2} (-1)^{i+j} g[(-1)^i r, (-1)^j s] \cos[m + (-1)^i r]\pi\xi \times \cos[n + (-1)^j s]\pi\eta + \tag{6a}$$

$$+ (1 - \bar{\nu}^2)\alpha^2 \sum_m \sum_n \bar{w}_{mn}\, \bar{g}_e(m,n) \sin m\pi\xi \sin n\pi\eta \tag{6b}$$

where the functions $g(t_1,t_2)$, $g_e(m,n)$ are defined as follows:

$$g(t_1,t_2) = \frac{mt_2(nt_1 - mt_2)}{(m+t_1)^4 + 2\varkappa\omega^2\alpha^2(m+t_1)^2(n+t_2)^2 + \omega^4\alpha^4(n+t_2)^4} \tag{7a}$$

$$\bar{g}_e(m,n) = \frac{\dfrac{\nu\bar{e}_x}{\delta_y\alpha^2} m^4 - (\bar{e}_x + \bar{e}_y) m^2 n^2 + \dfrac{\nu\bar{e}_y\alpha^2}{\delta_x} n^4}{m^4 + 2\varkappa\omega^2\alpha^2 m^2 n^2 + \omega^4\alpha^4 n^4}, \qquad \bar{e}_x = \frac{e_x}{t} \tag{7b}$$

2.3 Solution to the Equilibrium Equation

Let us solve the equation (1a) by GALERKIN´s method. The system of GALERKIN´s equations is then

$$\int_0^1 \int_0^1 X \sin p\pi\xi \sin q\pi\eta \, d\xi \, d\eta = 0, \quad (p = 1,2,3,\ldots; q = 1,2,3,\ldots) \tag{8}$$

After integration (8) is transformed in a system of algebraic cubic equations, which is solved by NEWTON-RAPHSON´s method. Details will be published in a journal.

3. NUMERICAL RESULTS

3.1 Critical Stress

The critical stress of an orthotropic plate is given by

$$\sigma_{cr,e} = \underbrace{\frac{\pi^2 E\psi}{12(\delta_x - \nu^2)\lambda^2\alpha^2}}_{\sigma_{cr}\,[1,9]} \cdot \left[1 + \underbrace{\frac{12\,\delta_y\alpha^2(1 + 2\varkappa\omega^2\alpha^2 + \omega^4\alpha^4)}{\psi(1-\bar{\nu}^2)} \cdot \bar{g}_e^2(m=1,\, n=1)}_{\text{influence of eccentricities } e_x, e_y}\right] \tag{9}$$

The influence of the stiffener eccentricity e_x ($e_y = 0$) on the critical stress is studied in the Tab. 1 on the four models.

Table 1	N1	N2	N4	N3
relative rigidity $(\psi - \bar{\psi})/\bar{\psi}$	5.214	0.533	0.058	-0.254
relative eccentricity e_x/t	5.600	2.560	1.524	0.990
ratio of stresses $\sigma_{cr,e}/\sigma_{cr}$	1.035	1.031	1.020	1.013

Details of the four large scale steel models N1, N2, N3, N4 (span 8.5m, depth 0.5125m) and of the test setup will be published in [4]. The full description of the tests can be found in [8].

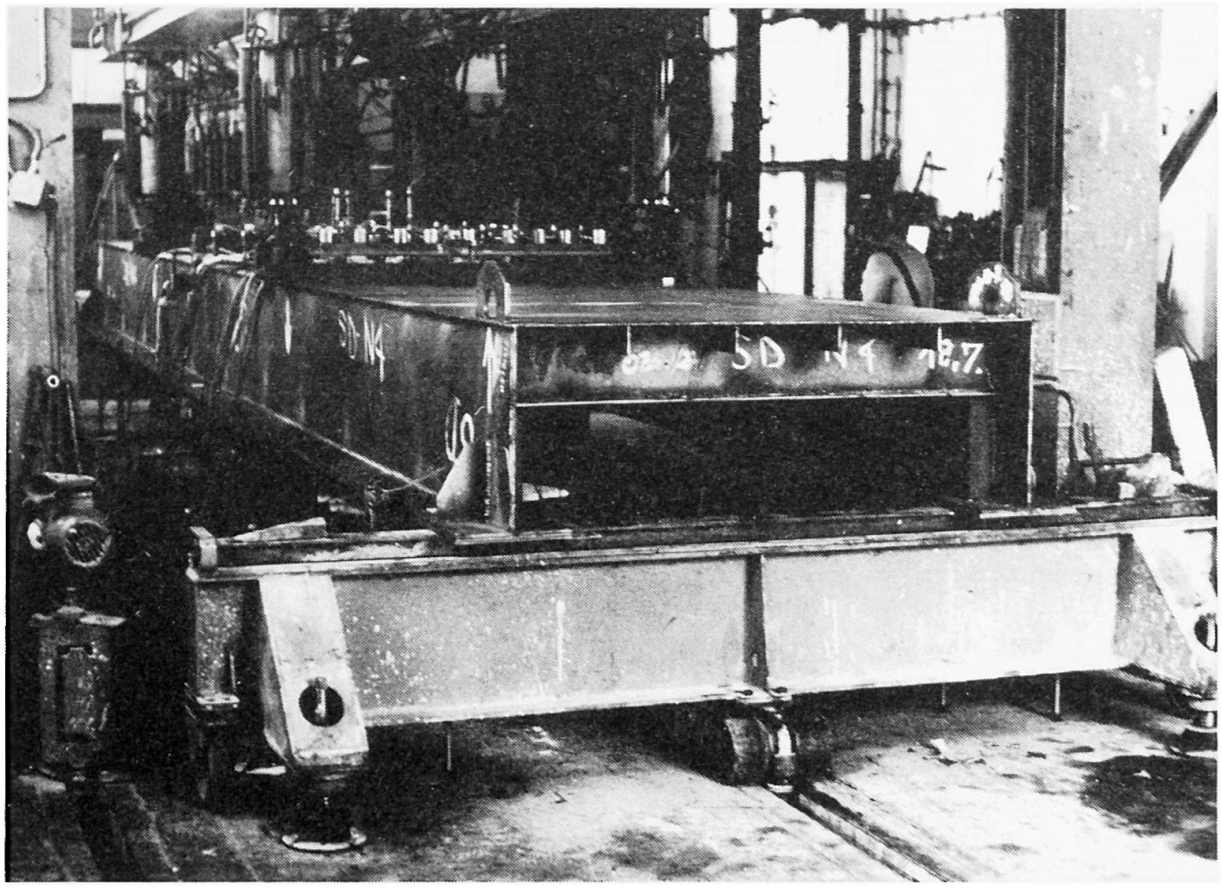

Fig. 1 KVOČÁK's test girder N4 [4,8]

3.2 Postcritical behaviour

The approach proposed in this paper enables to distinguish between two directions of orthotropic plate buckling: /i/ in the direction of the flange plate ($e_x < 0$) and /ii/ in the direction of the longitudinal stiffeners ($e_x > 0$). The former case is more danger (Tab. 2), but both cases differ only slightly from the case with $e_x = 0$. The results presented in the Tab.2 were calculated for one term of series (2), viz. w_{11}, w_{011} and they practically don't differ from those calculated for five terms of series (2), viz. w_{11}, w_{13}, w_{31}, w_{33}, w_{15} and w_{011}. $\bar{\sigma}_{x,e}$ ($e_x \neq 0$) and $\bar{\sigma}_x$ ($e_x = 0$) are the average stresses in the orthotropic plate at the moment when the maximum membrane stress attains the yield stress f_y. On the question of the in-plane boundary conditions of the orthotropic plate it had been assumed that transverse edges are "constrained", i.e. that they can freely move but remain straight. The longitudinal edges

can deflect in the plane of the plate.

Table 2		N1	N2	N4	N3
$\sigma_{cr,e}/f_y$		6.429	1.581	1.079	0.756
w_0/t		0.500	0.600	0.600	0.730
$\frac{\bar{\sigma}_{x,e}}{\bar{\sigma}_x}$	$e_x < 0$	0.990	0.986	0.902	0.856
	$e_x = 0$	1.	1.	1.	1.
	$e_x > 0$	1.008	1.012	1.057	1.134

4. CONCLUSIONS

The study have been started, which enables to evaluate the influence of the stiffener eccentricities e_x, e_y on the critical stress (Tab. 1) and/or on the limit load of the orthotropic plate in compression (Tab. 2). The first results of the study have shown that the basic system of non-linear equations (1) can be simplified by neglecting the terms that contain eccentricities e_x, e_y.

REFERENCES

1. BALÁŽ I.: Post-Critical Behaviour of Stiffened Compression Flanges and Torsion of Large Box Girder Bridges /in Slovak/. Ph.D. Thesis, Slovak Academy of Sciences, Bratislava 1977.

2. BALÁŽ I.: Ausgesteifte Druckgurte von Kastenträgerbrücken. Stahlbau, Mai 1987.

3. BALÁŽ I., DJUBEK J., MAQUOI R., MASSONNET Ch.: État limite des plaques orthotropes comprimées. Constr. Métallique, No.2, 1979.

4. BALÁŽ I., KVOČÁK V.: Traglastversuche an stählernen Kastenträgern mit längsausgesteiften Druckgurten. Stahlbau , in print.

5. DJUBEK J., KODNÁR R., ŠKALOUD M.: Limit State of the Plate Elements of Steel Structures. Birkhäuser Verlag, Basel-Boston-Stuttgart 1983.

6. DUBAS P., GEHRI E.: Behaviour and Design of Steel Plated Structures. Zürich, January 1986.

7. JETTEUR P.: Contribution à la solution de problèmes particuliers d´instabilité dans les grandes poutres métalliques. These de doctorat. Collection des publications de la Faculté des Sciences Appliquées, No,94, Univ. de Liège 1984.

8. KVOČÁK V.: Grenztragfähigkeit der Flächensysteme. Dissertation. Slowakische Technische Hochschule Bratislava, Košice 1987.

9. MAQUOI R., MASSONNET Ch.: Théorie non-linéaire de la resistance postcritique des grandes poutres en caisson raidies. Mémoires de l´AIPC, 31-II,1971.

On the Load Capacity of Stiffened Plate Girders

Sur la capacité portante des poutres à âme pleine raidie

Zur Regelung der Tragfähigkeit versteifter Blechträger

Joachim SCHEER
Civil Engineer
TU Carolo-Wilhelmina
Braunschweig, FRG

Joachim Scheer, born 1927, obtained his Ph.D. in 1958. As a Consulting Engineer he was involved in the design of bridges, masts and scaffolding. Since 1971 he has been a professor for Steel Structures, first in Hannover. and from 1976 in Braunschweig, working mainly on plate stability, masts and code development.

Hartmut PASTERNAK
Civil Engineer
TU Carolo-Wilhelmina
Braunschweig, FRG

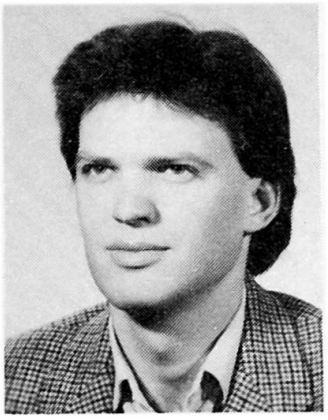

Hartmut Pasternak, born 1954, obtained his Ph.D. in 1981. As a research engineer he was involved in the design of industrial steel buildings, silos and cranes. Since 1986 he has been a research worker at the Institute of Steel Structures in Braunschweig, working on load capacity and load modelling problems.

SUMMARY
Since 1935 over 200 experiments on stiffened plate girders, subjected to shear and bending loads, have been carried out worldwide. It is now to be determined, using a probabilistic approach whether, by means of the above mentioned experiments, the tension field model of the Eurocode 3 is verified for transversely stiffened girders and whether it may be extended to longitudinally stiffened ones.

RÉSUMÉ
Depuis 1935, plus de 200 expériences ont été effectuées sur la capacité portante des poutres à âme pleine raidie, soumises à des efforts tranchants et fléchissants. L'objet de cette publication est de déterminer, de façon probabilistique, si le modèle de champ de traction de l'Eurocode 3 est vérifiable pour les poutres à âme pleine raidie transversalement et s'il peut être étendu aux poutres à âme pleine raidie longitudinalement, en tenant compte des expériences mentionnées auparavant.

ZUSAMMENFASSUNG
Weltweit wurden seit 1935 über 200 Versuche zur Tragfähigkeit ausgesteifter Vollwandträger unter Schub- und Biegebeanspruchung durchgeführt. Jetzt wird auf probabilistischer Grundlage untersucht, ob damit das Zugfeldmodell des Eurocode 3 für querversteifte Träger verifiziert und auf längsversteifte Träger ausgedehnt werden kann.

1. INTRODUCTION

In the past three decades, various tension field models were developed in order to predict the ultimate load capacity of stiffened plate girders subjected to shear and bending loads [1].

From time to time this development has been the target of fundamental questioning. Recently, a design model, based on the fully plastic shear load of the unstiffened web, has been presented [2].

Parallel to this, the number of experiments on stiffened plate girders has continually increased; in 1968, approximately 50 experiments were carried out, ten years later about 140 and nowadays there are more than 200.

However, experiment and theory only have their meaningfulness if full attention is paid to the stochastic character of the load capacity, and its influence quantities, in the experimental evaluation as well as in the calculations.

Since 1986, the Institute for Steel Structures in Braunschweig is working on the documentation, evaluation and recalculation of all available experiments. The work is performed - in an unprecedented extensive manner - using the programmable database system dbaseIII+. Moreover, it was attempted to estimate the uncertainty in the experiment execution and in the load capacity prediction.

In the context of the revision of the EC3, a few new questions arise, that may now be answered:

- is it allowable, in the Eurocode safety concept to apply the tension field models to transversely stiffened plate girders?
- could the application of these models, within the same safety concept, be extended to longitudinally stiffened girders? Which of the established models is optimal, taking into account the results of the experiments that were analysed in this study?

2. EVALUATION PROCEDURE

After compiling all experimental data into databases for transversely and longitudinally stiffened girders, the experiments containing parameters outside of the EC3 definition domain were rejected. The most frequent reason therefore were end post failures.

The test analysis described below (Fig. 1) was derived from the outline of the Eurocode paper "Procedure for the determination of the design resistance from tests" published in September 1987.

For the remaining i tests, the measured values of load capacities $V_{ue,i}$ (for the moment considered as exact), are compared with the calculated values $V_{ut,i}$ using model factors M_i, whose mean value $\bar{M}$ as well as the error terms δ_i are calculated. The scattering of the measured values with respect to the theoretical ones can be estimated by means of v_δ.

The variation coefficient v_{Vut} of the calculated load capacity is to be estimated from the randomization of the design models according to sections 3 and 4, in which the input values (basic variables) are to be formulated with variation coefficients normally used for steel structures:

yield stress	$- v_{fy}$	$= 0.06 \ldots 0.08$
modulus of elasticity	$- v_E$	$= 0.04$
plate thickness	$- v_t$	$= 0.02$

The authors have no data concerning the scattering of the buckling coefficient k_s (mainly because of the scattering of the boundary conditions). It is assumed that $v_{ks} = 0.03$. The scattering of the other input values is negligible. From the computational model, the variation coefficient of the load capacity is then calculated to be $v_{Vut} = 0.08$.

1. Measure $V_{ue,i}$
2. Calculate $V_{ut,i}$ (from EC3 or [1])
3. $M_i = \dfrac{V_{ue,i}}{V_{ut,i}}$
4. $\bar{M} = 1/n \Sigma M_i$
5. $\delta_i = \dfrac{M_i}{\bar{M}}$
6. $v_\delta = \sqrt{\dfrac{1}{n-1}\left(\sum_{i=1}^{n} \delta_i^2 - n \cdot 1\right)}$
7. Estimate v_{Vut}
8. Estimate $v_{\delta exp}$
9. $v_{Vu} = \sqrt{v_{Vut}^2 + v_\delta^2 - v_{\delta exp}^2}$
10. $V_{u,k} = \bar{M}\, V_{ut} \exp(-1{,}645\, v_{Vu} - 0{,}5\, v_{Vu}^2)$ for LN-distributed load capacity
11. $\gamma_m = \exp((0{,}8\,\beta - 1{,}645)\, v_{Vu})$, $\beta = 3{,}8$

Fig.1 Algorithm

Until now it has not been taken into account, that vaguely defined experimental data must also have been introduced into the data base: e.g. the yield stress was often not measured or measured inaccurately, the modulus of elasticity was often not measured at all, and in some cases, only the nominal plate thicknesses were given. The scattering for the whole set of experiments may be estimated with $v_{\delta exp} = 0.10$.

The variation coefficient v_{Vu}, characteristic value $V_{u,k}$ as well as the partial safety factor γ_m of the ultimate load capacity may then be calculated.

3. TRANSVERSELY STIFFENED GIRDERS

The EC3 contains simplifying assumptions for the load capacity calculations of transversely stiffened girders: bending moment and longitudinal force are taken up by the flange, transverse

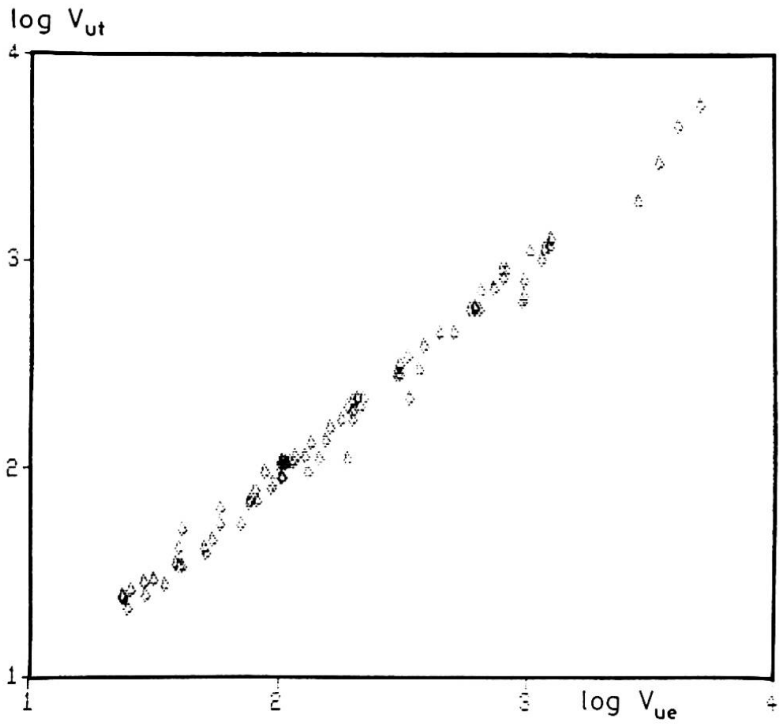

Fig.2 Correlation between calculation and experiment

forces are transfered to the web through the tension field and the shear field mechanism.

Fig.2 shows the satisfactory agreement between calculated and experimental results.

Fig.3 gives the frequency distribution of the model factor.

Characteristic value and partial safety factor of the load capacity may be read off Fig.4.

4. LONGITUDINALLY STIFFENED GIRDERS

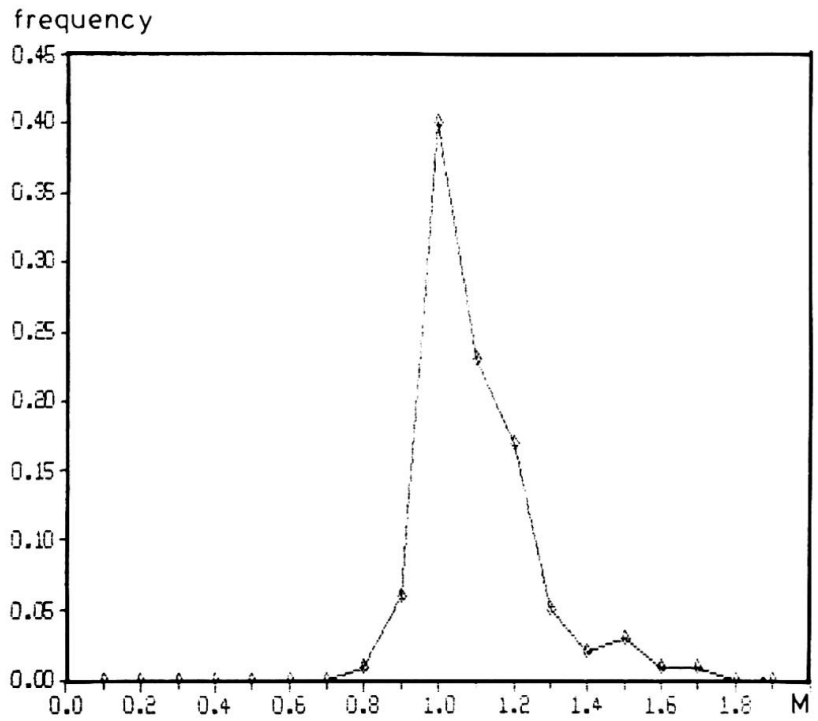

Fig.3 Frequency distribution of the model factor

The limit load capacity of longitudinally stiffened girders could be determined within EC3, in the same way as for transversely stiffened girders. The assumption of the tension field mechanism, however, still has to be determined. During the comparison of competing models, it was possible to substantially increase the number of evaluated experiments, relative to earlier investigations described in [1]. Fig.4 gives the results for various models.

	Transversely stiffened girders (n = 98)	Longitudinally stiffened girders (n = 59)			
		1	2	3	4
		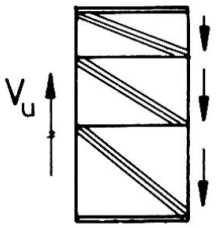	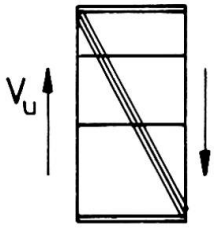	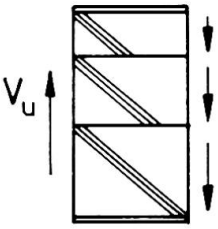	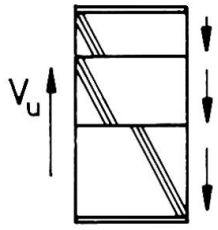
		Separate tension field bands Each a function of subpanel τ_i and aspect ratio α_i	Single tension field band A function of full panel aspect ratio α	Separate tension field bands Each a function of subpanel τ_i and common aspect ratio α_{min}	Separate tension field bands Each a function of subpanel τ_i and common panel aspect ratio α
$\bar{M}$	1,10	1,15	1,17	1,12	0,99
v_δ	0,16	0,13	0,10	0,12	0,08
$V_{u,k}$	0,85 V_{ut}	0,95 V_{ut}	0,94 V_{ut}	0,94 V_{ut}	0,91 V_{ut}
γ_m	1,23	1,17	1,12	1,16	1,08

Fig.4 Characteristics of various computational models

5. CONCLUSIONS

The first two questions of section 1 can in priciple be answered positively. However, the characteristic values of the load capacities are a few percent lower than the theoretical values; the partial safety factors are mostly greater than the code value of $\gamma_m = 1.1$.

Moreover, it is noticeable that even the models having an average model factor above 1, with consideration of all the scattering originating from experiment and calculation, do not lie on the safe side any more. Considering this result, one might be tempted to jump to conclusions, but should rather be prompted to further investigate the experimental assessment of computational models.

Model 2 seems to be optimal for describing the behaviour of longitudinally stiffened girders; the model is simpler and does not yield worse characteristics than the other models.

The method in [2] is characterized by scattering in the model factors, that is larger than that of the models discussed in section 3 and 4. From our experience, this yields a lower bound

of the load capacity.

All of the experimental data and detailed results of the evaluation are available from the authors.

6. ACKNOWLEDGEMENT

The Authors wish to thank the Federal Ministry of Civil Engineering for financial support, all scientists who have sent their research papers, as well as Mr. O. Kroth for his support in setting up the data base.

REFERENCES

1. Dubas P., Gehri E.: Behaviour and Design of Steel Plated Structures, ECCS publication n.44. Zurich 1986

2. Herzog M.: Tragfähigkeit und Bemessung unversteifter und versteifter Blechträger auf Schub in einfachster Näherung, Bauingenieur 63 (1988)

Analytical Model for Vibration of Y-Shaped Structure

Modèle analytique de la vibration de structures en forme de Y

Analytisches Vibrationsmodell für Y-förmige Bauwerke

Cuiru YANG
Civil Engineer
Build. Design Inst.
Xi'an, Shaanxi, China

Cuiru Yang, born 1940, received her Applied mechanics degree at the Xi'an Jiaotong university, Xi'an, Shaanxi, P.R.CHINA. For eighteen years she was engaged in design of civil and industrial buildings. Cuiru Yang now is involved in the research of aseismic design of buildings.

SUMMARY
Y-shaped buildings are characteristically non-orthogonal in the directions of structural elements and asymmetric in rigidity. For the Y-shaped building with a semirigid floor system, the longitudinal deformations of its wings, because of their lengths in plan and due to the much more rigid central "core", can be reasonably neglected. The "Spatial Multi-Mass-Point System" is used as the mechanical model to describe the various structural responses under ground motion, i.e. parallel translation, twisting and the deformations of the wings perpendicular to their longitudinal axes.

RÉSUMÉ
Les bâtiments en forme de Y sont, de façon caractéristique, non-orthogonaux dans la direction des éléments structuraux et asymétriques dans leur rigidité. Pour les bâtiments en forme de Y avec un système de plancher semi-rigide, les déformations longitudinales des ailes peuvent être raisonablement négligées en raison de leur longueur en plan et de la trop grande rigidité du noyau. Un modèle mécanique permet de décrire divers comportements structuraux sous l'effet de mouvements au sol, par exemple translation parallèle, torsion et déformation des ailes perpendiculairement aux axes longitudinaux.

ZUSAMMENFASSUNG
Im Grundriss Y-förmige Bauwerke weisen schiefwinklige Anschlüsse der Tragelemente und eine asymmetrische Steifigkeit auf. Bei der Verwendung von halbsteifen Deckensystemen können die Längsverformungen der Y-Flügel verglichen mit den Kernverschiebungen vernachlässigt werden. Ein räumliches Modell mit mehreren Masspunkten wird verwendet, um das Verhalten bei Bodenbewegung, d.h. die Verschiebungen, Verdrehungen und die Verbiegungen der Y-Flügel zu beschreiben.

1. INTRODUCTION

Few actual buildings are entirely symmetric with respect to mass and stiffness distribution about one or more axes of the buildings. This geometric and physical asymmetry is greatly enhanced with irregular shaped high-risers which have come into architectural vogue during the recent decades. Furthere more, floor systems which used to be taken as absolutely rigid diaphragms are now known in some cases that their rigidities are only comparable in magnitude (although often greater than) those of the vertical structural elements, i.e. floors are to some degree deformationable. Damage surveys of major earthquakes clearly reveal the unfavorable effects of asymmetry and floor deformation on some of the damaged buildings. It is therefore incumbent upon the structural engineer to pay serious attention to these facts in his seismic analysis and design of an important building, especially when it is irregular shaped in plan.

2. MATHEMATICAL MODEL

Before discussing the mathematical aspects of the structure's model, it is perhaps necessary to mention briefly the important physical property of the floor system. In recent years inverstigations have been carried out on this subject, some by observing the ambient vibrations of buildings, some by recording the deformed building subject to applied lateral loading. The results may be summarized as: (1) The magnitude of floor stiffness depends on the lenth-width ratio and the material and construction of flooring. (2) The shape of floor deformation is basically of the shear type. (3) The actual values of floor rigidity are difficult to determine and few reliably accurate figures have been given. For the common type of floors of precast concrete, the "basic" shear stiffness of 10^5 kN is often accepted.

Complex-shaped tall buildings are characteristically non-orthogonal in directions of structural elements, asymmetric in rigidity and the lack of coincidence between the dominant direction of ground motion and one of the principal axes of symmetry, thus resulting in strong torsional vibrations during an earthquake. If the building is long and narrow in plan, or the flooring is comparatively flexible, its horizontal deformation is appreciable. An adequate analysis should take all the above facts in consideration.

The establishment of the mathematical model is best illustrated by taking an example. The Y-shaped high-riser is quite popular today. If the wings are short compared to their width, and if the concrete floors are cast-in-situ, the structure may be regarded as a "multiple rigid disk system" for analysis purpose. If , however, the wings are long and narrow, or if the flooring is less rigid, for example, like the precast slab type, or, if the lateral stiffnesses of the vertical structure elements of the wings are much less than that of the central core, then the influence of floor deformation should not be neglected.

For the Y-shaped tall building as shown in Fig.1, the longitudinal deformations of its wings, because of their lengths in plan and due to the much more rigid central "core" can be reasonnally neglected. The "Spatial Multi-mass-point System" (Fig.2) is used as the mathematical model to describle the structural various responses under ground motion, i.e. parallel translation, twisting and the deformations of the wings perpendicular to their longitudinal axes.

2. EQUATIONS OF MOTION

We can assume the dominant components of a very complex earthquake ground motion are the two-directional translations plus rotation. The equations of motion of the system under an earthquake may be written in the familiar form:

$$[M]\{\ddot{U}\} + [C]\{\dot{U}\} + [K]\{U\} = -[M]\{\ddot{U}_g\} \qquad (1)$$

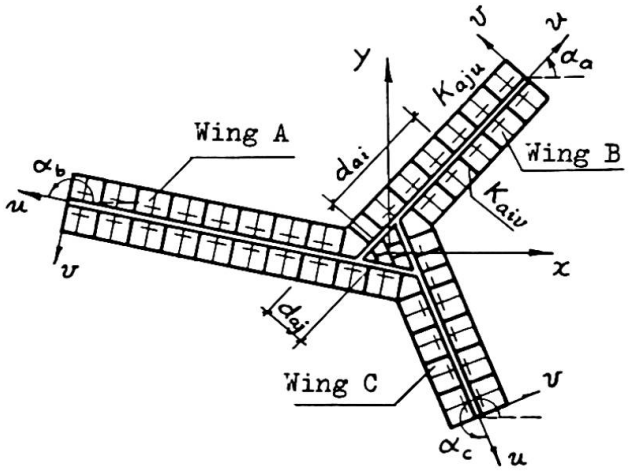

Fig.1 Typical floor plan

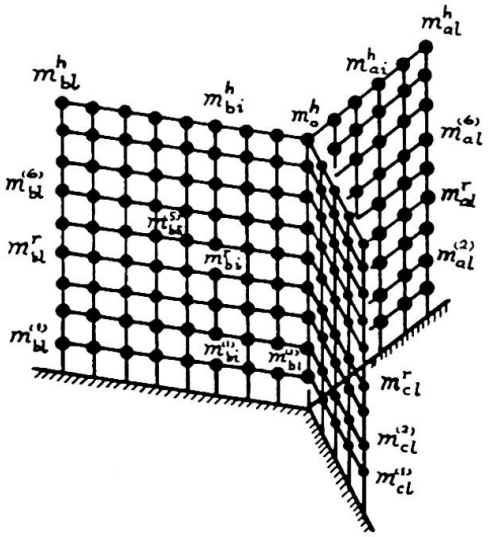

Fig.2 Mechanical model

$$\{U\} = \left[\{x_o\}^T \quad \{y_o\}^T \quad \{\varphi\}^T \quad \{v\}^T\right]^T ,$$

$$\{\ddot{U}g\} = [I][\ddot{x}_g \quad \ddot{y}_g \quad \varphi_g \quad 0\ ]^T ,$$

$$[I] = \mathrm{diag}\left[\{1\}_h \quad \{1\}_h \quad \{1\}_h \quad \{1\}_{(l+\sum_s lh)}\right] ,$$

where $\{U\}$, $\{\dot{U}\}$, $\{\ddot{U}\}$ are respectively the column vectors of the generalized relative displacements, velocities and accelerations. $\{\ddot{U}g\}$ is column vector of the generalized ground acceleration. $\{x_o\}$, $\{y_o\}$ and $\{\varphi\}$ give respectively the x, y, φ directional translations in the global co-ordinates. $\{v\}$ gives the displacements due to floor deformation (Fig.3).

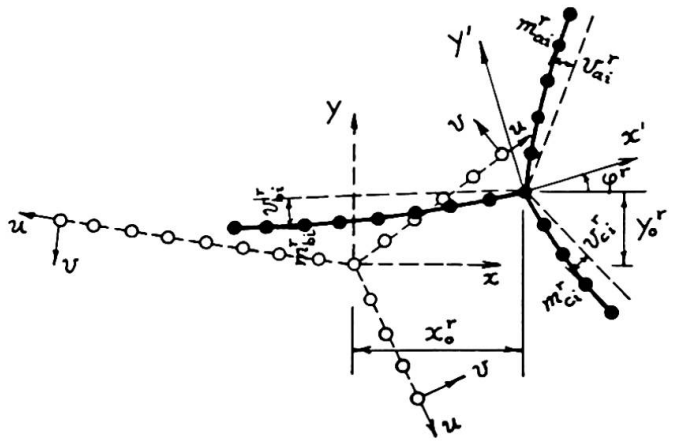

Fig.3 Displacements of the rth floor's mass-points

[M] is the generalized mass matrix, in which [m], [J] are respectively submatrices of mass and mass moment of inertia. $[m_{vx}]$, $[m_{vy}]$ and $[m_{v\varphi}]$ are the coupled mass submatrices between the translations and rotation.

[K] and $[K_{UV}]$ are respectively the stiffness matrices in the global and local co-ordinates, in which [T] is the transformation matrix. $[K_U]$, $[K_V]$ and $[K_\varphi]$ are the stiffness matrices refferred to the planar motion of the rigid disk system. $[K_{VV}]$ is the stiffness matrix of the flexible floor system. $[K_v]$ is the

stiffness matrix of the vertical structural elements, $[k_v]$ is the stiffness matrix coupling the vertical sub-structures due to stiffness of diaphragms. $[K_{vV}]$ and $[K_{v\varphi}]$ are the stiffness matrices coupling the displacements due to floor deformation and those due to solid-body motion of the floors. $[d_v]$ and $[d_u]$ are the matrices giving the distances between the story mass centers of the wings to the story mass center of the building. $k_{si}^{r,r}$ is the equivalent horizontal shearing stiffness of the floor of the ith bay.

$$\{x_o\} = \left[\, x_o^{(1)} \quad x_o^{(2)} \cdots x_o^t \cdots x_o^h \,\right]^T , \quad \{y_o\} = \left[\, y_o^{(1)} \quad y_o^{(2)} \cdots y_o^t \cdots y_o^h \,\right]^T ,$$

$$\{\varphi\} = \left[\, \varphi^{(1)} \quad \varphi^{(2)} \cdots \varphi^t \cdots \varphi^h \,\right]^T , \quad \{v\} = \left[\, \{0\}^T \quad \{v_a\}^T \quad \{v_b\}^T \quad \{v_c\}^T \,\right]^T ,$$

$$\{v_s\} = \left[\, \{v_{s1}\}^T \quad \{v_{s2}\}^T \cdots \{v_{si}\}^T \cdots \{v_{sl}\}^T \,\right]^T , \quad (s = a,b,c)$$

$$\{v_{si}\} = \left[\, v_{si}^{(1)} \quad v_{si}^{(2)} \quad \cdots \quad v_{si}^t \quad \cdots \quad v_{si}^h \,\right] , \quad (i = 1,2,\cdots,l)$$

$$M = \begin{bmatrix} [m] & [0] & [0] & [m_{xv}] \\ [0] & [m] & [0] & [m_{yv}] \\ [0] & [0] & [J] & [m_{\varphi v}] \\ [m_{vx}] & [m_{vy}] & [m_{v\varphi}] & [m_v] \end{bmatrix} , \quad [m] = \mathrm{diag}\left[\, m^{(1)} \quad m^{(2)} \cdots m^r \cdots m^h \,\right] ,$$

$$[J] = \mathrm{diag}\left[\, J^{(1)} \quad J^{(2)} \cdots J^r \cdots J^h \,\right] ,$$

$$[m_v] = \mathrm{diag}\left[\, [0] \quad [m_a] \quad [m_b] \quad [m_c] \,\right] ,$$

$$[m_s] = \mathrm{diag}\left[\, [m_{s1}] \quad [m_{s2}] \cdots [m_{si}] \cdots [m_{sl}] \,\right] ,$$

$$[m_{si}] = \mathrm{diag}\left[\, m_{si}^{(1)} \quad m_{si}^{(2)} \cdots m_{si}^t \cdots m_{si}^h \,\right] , \quad (s = a,b,c)$$

$$[m_{vx}] = -[m_v][\bar{I}]\{S\} , \quad [m_{vy}] = [m_v][\bar{I}]\{C\} , \quad [m_{yv}] = [m_{vy}]^T ,$$

$$[m_{xv}] = [m_{vx}]^T , \quad [m_{v\varphi}] = [m_v][d_i][\bar{I}]\{1\} , \quad [m_{\varphi v}] = [m_{v\varphi}]^T ,$$

$$\{S\} = [\sin\alpha_a \quad \sin\alpha_a \quad \sin\alpha_b \quad \sin\alpha_c] ,$$

$$\{C\} = [\cos\alpha_a \quad \cos\alpha_a \quad \cos\alpha_b \quad \cos\alpha_c] ,$$

$$[\bar{I}] = \mathrm{diag}\left[\, \{1\}_l \quad \{1\}_l \quad \{1\}_l \quad \{1\}_l \,\right] , \quad \{1\} = [1 \quad 1 \quad 1 \quad 1] ,$$

$$[d_i] = \mathrm{diag}\left[\, [0] \quad [d_a] \quad [d_b] \quad [d_c] \,\right] ,$$

$$[d_s] = \mathrm{diag}\left[\, [d_{s1}] \quad [d_{s2}] \cdots [d_{si}] \cdots [d_{sl}] \,\right] ,$$

$$[d_{si}] = \mathrm{diag}\left[\, d_{si}^{(1)} \quad d_{si}^{(2)} \cdots d_{si}^t \cdots d_{si}^h \,\right] , \quad (s = a,b,c)$$

$$[K] = \begin{bmatrix} [K_{xx}] & [K_{xy}] & [K_{x\varphi}] & [K_{xv}] \\ [K_{yx}] & [K_{yy}] & [K_{y\varphi}] & [K_{yv}] \\ [K_{\varphi x}] & [K_{\varphi y}] & [K_{\varphi\varphi}] & [K_{\varphi v}] \\ [K_{vx}] & [K_{vy}] & [K_{v\varphi}] & [K_{vv}] \end{bmatrix} = [T]^T [K_{UV}][T] ,$$

$$[K_{UV}] = \begin{bmatrix} [K_U] & [0] & [K_{U\varphi}] & [0] \\ [0] & [K_V] & [K_{V\varphi}] & [K_{Vv}] \\ [K_{\varphi U}] & [K_{\varphi V}] & [K_\varphi] & [K_{\varphi v}] \\ [0] & [K_{vV}] & [K_{v\varphi}] & [K_{vv}] \end{bmatrix} , \quad [T] = \begin{bmatrix} \{C\}_4 & \{S\}_4 & \{0\} & [0] \\ \{S\}_4 & -\{C\}_4 & \{0\} & [0] \\ \{0\} & \{0\} & \{1\}_4 & [0] \\ \{0\} & \{0\} & \{0\} & [I]_{4x4} \end{bmatrix}$$

$$[K_U] = \mathrm{diag}\left[\, [K_{ou}] \quad [K_{au}] \quad [K_{bu}] \quad [K_{cu}] \,\right] ,$$

$$[K_V] = \mathrm{diag}\left[\, [K_{ov}] \quad [K_{av}] \quad [K_{bv}] \quad [K_{cv}] \,\right] ,$$

$$[K_\varphi] = \left[\, [d_v] \quad [d_u] \,\right] \begin{bmatrix} [K_U] & [0] \\ [0] & [K_V] \end{bmatrix} \begin{Bmatrix} [d_v] \\ [d_u] \end{Bmatrix} , \quad [K_{\varphi U}] = -[d_v][K_U] , \quad [K_{\varphi V}] = [d_u][K_V] ,$$

$$[d_v] = \mathrm{diag}\left[\, [d_{ov}] \quad [d_{av}] \quad [d_{bv}] \quad [d_{cv}] \,\right] ,$$

$$[d_u] = \mathrm{diag}\left[\, [d_{ou}] \quad [d_{au}] \quad [d_{bu}] \quad [d_{cu}] \,\right] ,$$

$$[d_{sv}] = \mathrm{diag}\left[\, d_{sv}^{(1)} \quad d_{sv}^{(2)} \cdots d_{sv}^t \cdots d_{sv}^h \,\right] ,$$

$$[d_{su}] = \mathrm{diag}\,[\,d_{su}^{(1)} \quad d_{su}^{(2)} \cdots d_{su}^{t} \cdots d_{su}^{h}\,]\ ,\quad (s = 0, a, b, c)$$

$$[K_{\varphi U}] = -[d_v][K_U]\ ,\quad [K_{\varphi v}] = [d_u][K_V]\ ,\quad [K_{U\varphi}] = [K_{\varphi U}]^T\ ,$$

$$[K_{vv}] = [K_v] + [k_v]\ ,\quad [K_v] = \mathrm{diag}\,[[0] \quad [K_{av}] \quad [K_{bv}] \quad [K_{cv}]]\ ,$$

$$[K_{sv}] = \mathrm{diag}\,[[K_{s1v}] \quad [K_{s2v}] \cdots [K_{siv}] \cdots [K_{slv}]]\ ,\quad (s = a, b, c)$$

$$|K_{siv}| = \begin{bmatrix} K_{siv}^{1,1} & K_{siv}^{1,2} & \cdots & K_{siv}^{1,t} & \cdots & K_{siv}^{1,h} \\ K_{siv}^{2,1} & K_{siv}^{2,2} & \cdots & K_{siv}^{2,t} & \cdots & K_{siv}^{2,h} \\ \cdots & \cdots & \cdots & \cdots & \cdots & \cdots \\ K_{siv}^{r,1} & K_{siv}^{r,2} & \cdots & K_{siv}^{r,t} & \cdots & K_{siv}^{r,h} \\ \cdots & \cdots & \cdots & \cdots & \cdots & \cdots \\ K_{siv}^{h,1} & K_{siv}^{h,2} & \cdots & K_{siv}^{h,t} & \cdots & K_{siv}^{h,h} \end{bmatrix}\ ,$$

$$[k_v] = \mathrm{diag}\,[[0] \quad [k_a] \quad [k_b] \quad [k_c]]\ ,$$

$$[k_s] = \begin{bmatrix} [k_{s1}]+[k_{s2}] & -[k_{s2}] & & & & \\ -[k_{s2}] & [k_{s2}]+[k_{s3}] & -[k_{s3}] & & 0 & \\ & \cdots & \cdots & \cdots & & \\ & & -[k_{si}] & [k_{si}]+[k_{s(i+1)}] & -[k_{s(i+1)}] & \\ & & & \cdots & \cdots & \cdots \\ & 0 & & & -[k_{s(l-1)}] & [k_{s(l-1)}]+[k_{sl}] & -[k_{sl}] \\ & & & & & -[k_{sl}] & [k_{sl}] \end{bmatrix}$$

$$[k_{si}] = \mathrm{diag}\,[\,k_{si}^{1,1} \quad k_{si}^{2,2} \quad k_{si}^{r,r} \quad k_{si}^{h,h}\,]\ ,\quad (s = a, b, c)$$

$$[K_{vV}] = [K_v][\bar{I}]\ ,\quad [K_{v\varphi}] = [K_v][d_i][\bar{I}]\ ,$$

$$[K_{Vv}] = [K_{vV}]^T\ ,\quad [K_{\varphi v}] = [K_{v\varphi}]^T\ ,$$

3. ANALYSIS AND COMPUTATION

The solution of the dynamic equation

$$[U][A] = [\lambda][A] \tag{2}$$

where $[U]$ stands for $[K]^{-1}[M]$, $[A]$ the total modal matrix and $[\lambda]$ the eigen value diagonal matrix, is trivial. $[\lambda]$ and $[A]$ give all the natural periods of vibration and modal shapes, while the participation factors of modes can be determined by simply inverting $[A]$, i.e.

$$[\Gamma] = [A]^{-1}[I] \tag{3}$$

$$\begin{bmatrix} \gamma_{x1} & \gamma_{y1} & \gamma_{\varphi 1} & \gamma_{v1} \\ \cdots & \cdots & \cdots & \cdots \\ \gamma_{xj} & \gamma_{yj} & \gamma_{\varphi j} & \gamma_{vj} \\ \cdots & \cdots & \cdots & \cdots \\ \gamma_{xN} & \gamma_{yN} & \gamma_{\varphi N} & \gamma_{vN} \end{bmatrix} = [A]^{-1} \begin{bmatrix} \{1\}_h & & & \\ & \{1\}_h & 0 & \\ & & \{1\}_h & \\ & 0 & & \{1\}_{(1+\sum_s l_s h)} \end{bmatrix}$$

$$[A] = [\{A_1\} \quad \{A_2\} \cdots \{A_j\} \cdots \{A_N\}]\ ,\qquad N = 3h + 1 + \sum_s l_s h$$

$$\{A_j\} = [\{X_j\}^T \quad \{Y_j\}^T \quad \{\Phi_j\}^T \quad \{V_j\}^T]$$

$$= [\,X_o^{(1)} \quad X_o^{(2)} \cdots X_o^h \mid Y_o^{(1)} \quad Y_o^{(2)} \cdots Y_o^h \mid \Phi^{(1)} \quad \Phi^{(2)} \cdots \Phi^h \mid$$

$$0 \quad V_{a1}^{(1)} \quad V_{a1}^{(2)} \cdots V_{a1}^h \cdots V_{ai}^{(1)} \cdots V_{ai}^h \cdots V_{al}^{(1)} \cdots V_{al}^h \quad V_{b1}^{(1)} \cdots$$

$$V_{b1}^h \cdots V_{bl}^{(1)} \cdots V_{bl}^h \cdots V_{c1}^{(1)} \cdots V_{c1}^h \cdots V_{cl}^{(1)} \cdots V_{cl}^h\,]$$

The resultant sideways of the jth mode of the vertical structural elements in

the local (or member) co-ordinates are derived from the generalized displacements of the structure by means of co-ordinate transformation. The jth earthquake forces acting on the vertical elements as isolated members are given by multiplying the displacement matrices by the corresponding stiffness matrices. The members' design internal forces are finally obtained by superposing all the modal contributions according to the CQC (complete quadratic combination) method.

4. CONCLUSIONS

When torsion and floor deformation are considered the foundamental period of the vibration of the irregular shaped building is about 5 % greater, the increase of the internal forces of the verticle elements far away from the central core may amount to as much as 20~90 % . For buildings of large foundamental periods , the first 15 modes should be taken in to account. For this reason, the CQC method is more accurate than commonly used SRSS method and the discrepency between the two is known to be approximate 10 % .

REFERENCES

1. Bao Zhiwen, Lai Jinyan, Microtremor Signal Analysis of the Buildings. Earthquake Engineering and Engineering Vibration, Sept. 1981. (in chinese)

2. Dahai LIU, Cuiru YANG, Xigen ZHONG, A Differential Translation-torsion Coupling Earthquake Response Analysis for Multi-story Factory Buildings. China Civil Engineering Journal, Dec. 1983.

3. E.L. Wilson, A. Der Kiureghian, E.P.Bayo, A Replacement for the SRSS Method in Seismic Analysis, Earthquake Engineering and Structural Dynamics, Vol. 9, 187-194 (1981).

4. Dahai LIU, Xigen ZHONG, Cuiru YANG, Aseismic Design of Buildings, 1st edition , Shaanxi Scientific Publishing House, P.R. CHINA, 1985.

Excitation Damping of Reinforced Concrete under Cyclic

Capacité d'amortisement du béton armé sous des charges cycliques

Zur Dämpfung von Stahlbeton unter zyklischer Belastung infolge Verbundhysterese

Gert KÖNIG
Prof. Dr.-Ing.
Technische Hochschule, Darmstadt,
Darmstadt, Bundesrep.
Deutschland

Gert König, geboren 1934, studierte an der TH Darmstadt Bauingenierwesen und erwab 1960 das Diplom. Seit 1971 ist er beratender Ingenieur VBI, seit 1972 Prüfingenieur für Baustatik. 1975 wurde er an die Technische Hochschule Darmstadt berufen. Er beschäftigt sich mit Hochhäusern aus Stahlbeton, dem Spannbetonbrückenbau, der Baudynamik, sowie mit den Grundlagen der Massivbauweise.

Ekkehard FEHLING
Dipl.-Ing.
Technische Hochschule, Darmstadt,
Darmstadt, Bundesrep.
Deutschland

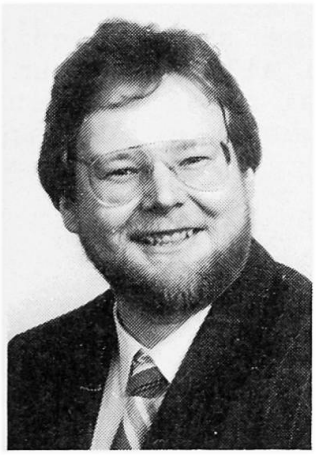

Ekkehard Fehling, geboren 1959, studierte an der TH Darmstadt Bauingenieurwesen und erwarb 1983 das Diplom. Seit 1983 Tätigkeit als wissenschaftlicher Mitarbeiter am Institut für Massivbau.

SUMMARY
The damping behaviour of reinforced concrete significantly influences the deformations of reinforced concrete structures under dynamic loading. The energy dissipation mechanisms due to cyclic bond action are studied experimentally and analytically. Results of theoretical models are compared with experimental data.

RÉSUMÉ
La capacité d'amortisement du béton armé influence de façon considérable les déformations des structures en béton armé sous l'effet de charges dynamiques. Les mécanismes de l'énergie de dissipation résultant de l'action d'adhérence cyclique sont étudiés de façoin expérimentale et analytique. Les résultats des modèles théoriques sont comparés avec les mesures faites.

ZUSAMMENFASSUNG
Die Dämpfungsfähigkeit des Stahlbetons kann die Verformungen von Stahlbetontragwerken unter dynamischer Belastung stark beeinflussen. Die Energiedissipation infolge Verbundhysterese liefert im gerissenen Zustand einen wichtigen Beitrag zur Dämpfung. Hier sollen die Ergebnisse diesbezüglicher experimenteller und analytischer Untersuchungen vorgestellt werden.

1. INTRODUCTION

The dynamic response of structures is influenced to a large extent by the damping behaviour of its structural elements. Especially in the cases of forced steady state-vibration and earthquake action a realistic estimate of damping, which should be regarded as a consequence of energy dissipation, is necessary in order to predict the peak response correctly.

In the following some basic considerations are presented which might help to understand and model one of the basic dissipative mechanisms in reinforced concrete: the hysteretic bond action between reinforcement and concrete. This mechanism is one of the main important sources for damping of R/C under service load conditions, where the reinforcing steel remains still elastic.

2. DAMPING AS A CONSEQUENCE OF ENERGY DISSIPATION

A Definition of Damping may be given by the damping ratio d:

$$d = D / W_p$$

where D denotes the Energy dissipated during one cycle and W_p means the Deformation-Energy (see Fig.1 and [1,2]). It is useful to define the deformational energy using the secant modulus and the Force

$$F_0 = (F_{max} + F_{min})/2,$$

which corresponds to the static equilibrium state as shown in Fig. 1. This definition allows to sum up or integrate D and W_p over different structural parts or volumina and interfaces. So the influence of each possible dissipative mechanism may be considered.

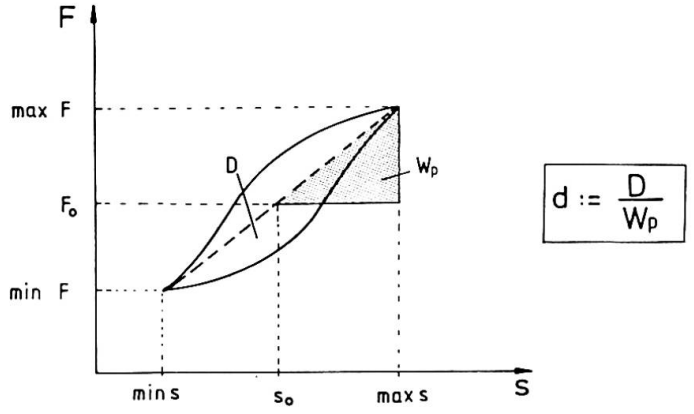

Fig. 1:
Definition
of Damping Ratio d

3. DISSIPATIVE MECHANISMS IN REINFORCED CONCRETE STRUCTURES

Energy Dissipation in R/C members is mainly caused by the following mechanisms:

- hysteresis of stress-strain-relationship of concrete,
- hysteresis of stress-strain-relationship of reinforcing steel,
- tensile fracture of concrete,
- hysteretic action of aggregate interlock in cracks,
- friction between aggregates and/or hardened cement paste in cracks, which open and close during load cycles,
- hysteresis of bond between reinforcing steel and concrete.

4. EXPERIMENTAL PARAMETRIC STUDY

In order to study the influence of hysteretic bond action upon energy dissipation in R/C-members an experimental program was set up. It was intended to let the experiments reveal the contribution of bond hysteresis to damping only and separate or exclude other dissipation mechanisms. So contrary to tests with beams or cantilever elements reported by [1,2,3] the test specimens used here only represent the region between two adjacent cracks in a R/C structural member (see Fig. 2). The load is applied directly via the rebar. The parameters under investigation are:

- rebar diameter,
- reinforcement percentage,
- concrete strength,
- crack spacing (i.e. length of specimen),
- preloading (i.e. maximum steel stress reached before and number of cycles),
- actual loading (i.e. max. and min. steel stress during actual cycle),
- excitation frequency.

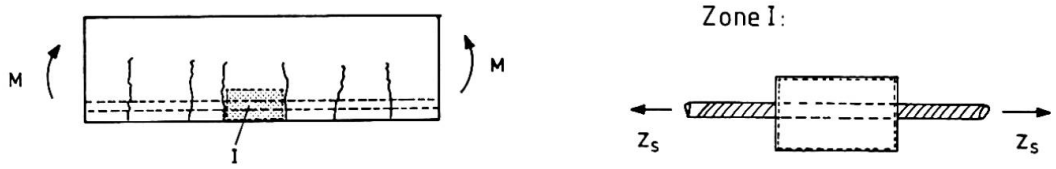

Fig. 2: Choice of specimen

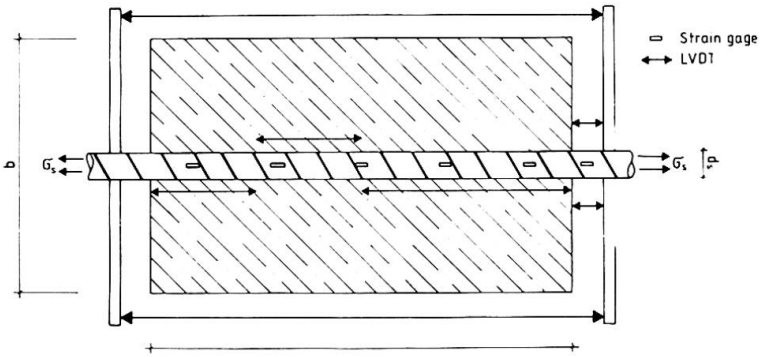

Fig. 3: Instrumentation of specimen

5. EVALUATION OF TEST DATA

On the basis of the measured longitudinal steel strain at the locations of the gages and the deformations measured by the LVDTs (see Fig.3) the - local steel stresses $\sigma_s(x)$,
- the local bond stresses $\tau_s(x)$ and
- the local slip $s(x)$

can be calculated.

6. PRELIMINARY RESULTS

Whereas in the first cycles a large increase of deformation occurs, the deformation tends to stabilize after a higher number of cycles. Fig. 4 shows an example of the bond stress-slip relation. Whereas for small bond stresses a friction-like-behaviour applies, for larger bond stresses a combination of elastic and plastic effects has to be considered.

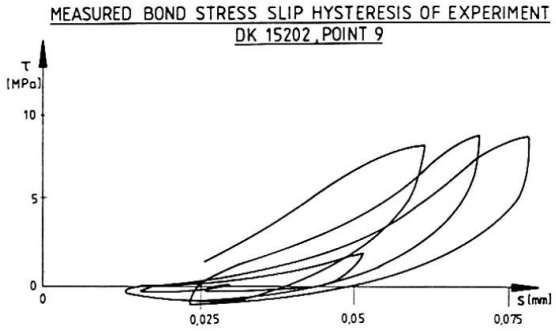

Fig. 4: Example of bond-stress-slip relation

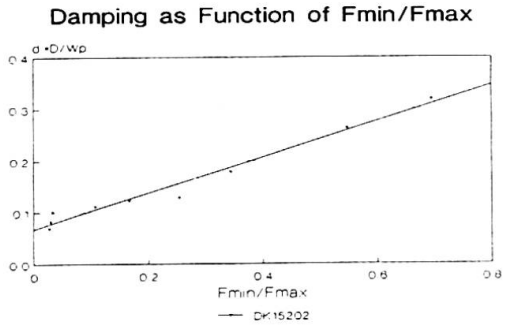

Fig. 5: Damping ratio d as function of F_{min}/F_{max} for max σ_s = 200 MPa

Fig. 5 shows the damping ratio d as a function of the ratio of minimum to maximum Force. For a large ratio F_{min}/F_{max}, this means, that for small oscillation amplitudes compared to the average Force F_0 the damping ratio d is higher than for small values of F_{min}/F_{max}. The damping ratio increases with crack spacing. This is a consequence of the large percentage of deformational energy of bond compared to the deformational energy in the steel. Vice versa this means that e.g. for high reinforcement percentages low damping values can be expected.

7. MODELING

In order to model the damping and stiffness behaviour of cracked R/C subjected to cyclic (tensile) load two steps are necessary:
- calculate the crack spacing,
- simulate bond action under cyclic loading for given crack pattern.

For the calculation of crack spacings the basic principles are reported in [5]. In order to simulate the bond action under cyclic loading the relation between bond stress and slip is needed as constitutive relation. Because of the fact that the bond law is influenced by many parameters which are not easy to estimate (e.g. self induced stress, dependancy from local discontinuities) simple bond models should be used.

For fully numerical calculations the model described in [6] may be used in the modified formulation [7] (Fig.6). It has been implemented into a nonlinear Finite-Element-Program as constitutive relation for contact elements [7] enabling a discrete crack approach.

MODELING OF BOND-STRESS-SLIP-RELATION

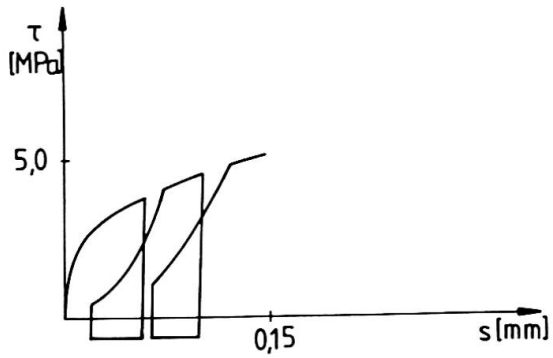

Fig. 6: Modified Bond Model after [6,7]

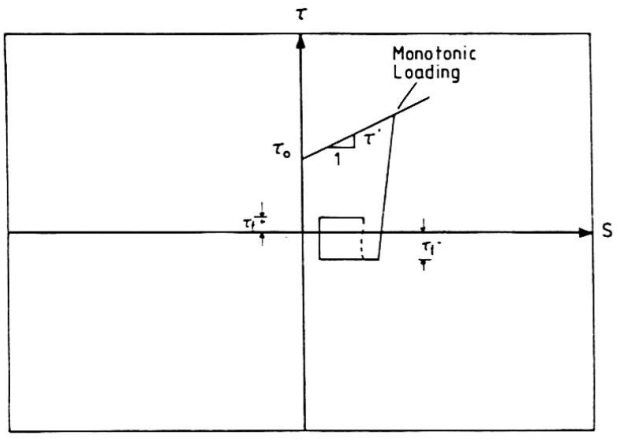

Fig. 7: Simplified Bond Law

For analytical treatment a simplified bond model can be adopted (Fig. 7). This enables a direct calculation of $\tau_s(x)$ and $\sigma_s(x)$, as Fig. 8 illustrates. Also the mean strain ε_{sm}, the crack width w and the deformational energy as well as the dissipated energy can be calculated directly. Fig. 10 gives the damping ratio calculated on the basis of a bond law as shown in Fig. 7. Also the tension stiffening effect for cyclic loading can be computed on this basis. Fig. 9 shows calculated deformations for axial tension.

By this method the energy dissipation due to bond can be calculated for R/C-members rather fast. Furthermore the proposed method is well suited to be used as subroutine in nonlinear Finite Element codes in order to model the hysteretic behaviour of reinforcement embedded in concrete by a smeared crack approach.

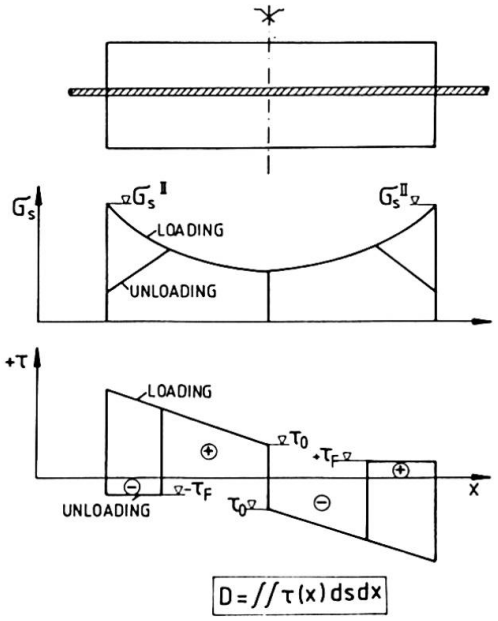

Fig. 8: Direct Calculation of $\sigma_s(x)$ and $\tau_s(x)$ for repeated loading

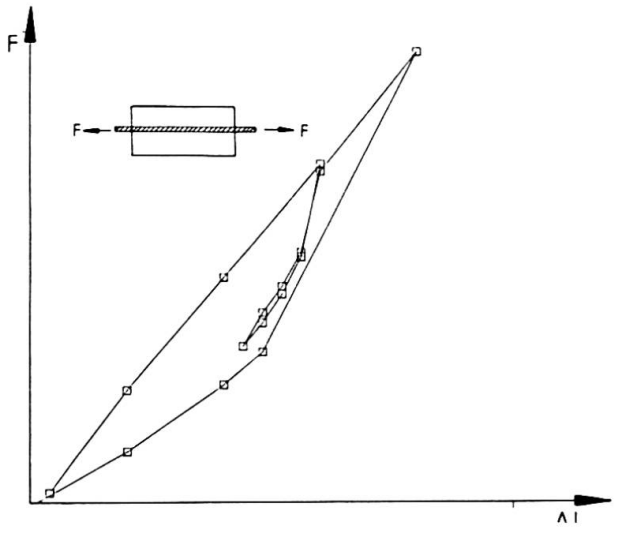

Fig. 9: Computed Force - Elongation - Relationship

Fig. 10: Computed Damping Ratio

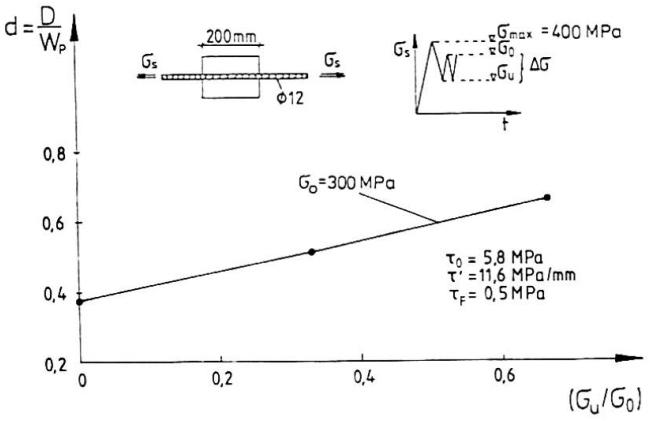

8. CONCLUSIONS

Energy dissipation due to hysteretic bond action plays an important role in respect to damping of R/C - structures under service load conditions. The experiments have shown the large influence of actual and previous loading on stiffness and damping behaviour. All parameters influencing the crack spacings will influence the damping ratio also. For modeling a numerical and an analytical procedure are discussed. Whereas both of them can be used with Finite Element Codes, the analytical approach also enables quick estimates of damping values with only few computational effort.

REFERENCES:

[1] Bachmann H., Dieterle R.: Versuche über den Einfluß der Rißbildung auf die dynamischen Eigenschaften von Leichtbeton- und Betonbalken, Bericht Nr. 75011-1, 1979, Institut für Baustatik und Konstruktion, ETH Zürich.

[2] Dieterle, R.: Modelle für das Dämpfungsverhalten von schwingenden Stahlbetonträgern im ungerissenen und gerissenen Zustand, Institut für Baustatik und Konstruktion, ETH Zürich, Bericht Nr. 111, April 1981.

[3] Ötes, A.: Zur werkstoffgerechten Berechnung der Erdbebenbeanspruchung in Stahlbetontragwerken, Mitteilung aus dem Institut für Massivbau der THD, Heft 25, Ernst & Sohn, Berlin 1984.

[4] Winter, S.: Versuche zur Dämpfung von Stahlbetonbauteilen infolge Verbundhysterese, Vertieferarbeit, Institut für Massivbau, TH Darmstadt, 1986/1987.

[5] Fehling, E., König, G., Scheidler, D.: Crack width control and Tension Stiffening, Darmstadt Concrete, Vol. 1, 1986.

[6] Ciampi, E., Eligehausen, R., Bertero, V.V., Popov, E.: Analytical Model for Concrete Anchorages of Reinforcing Bar under Generalized Excitation, Report No. UCB/EERC-82/23, Nov. 1982, Earthquake Engineering Research Center, University of California.

[7] Tue, N.: Zur Spannungsumlagerung im Spannbeton bei der Rissbildung, Diplomarbeit, Darmstadt 1987.

Computer Analysis of Inelastic Behavior of Reinforced Concrete Frame

Analyse par ordinateur du comportement inélastique d'un cadre en béton armé

Computeranalyse des inelastischen Verhaltens von Stahlbetonrahmen

Seiji KOKUSHO
Dr.Eng., Prof.
Tokyo Inst. of Techn.
Tokyo, Japan

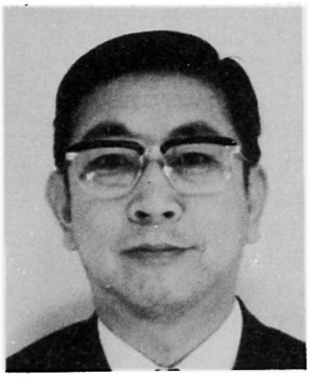

Seiji Kokusho, born in 1927, received his Dr.Eng. in 1961 from University of Tokyo. The objective of his research is to establish the rational ultimate design method of reinforced concrete structure with sufficient aseismic safety.

Akira WADA
Dr.Eng., Assoc. Prof.
Tokyo Inst. of Techn.
Tokyo, Japan

Akira Wada, born in 1946, received his Dr.Eng. in 1981 from the Tokyo Inst. of Tech. His research interests include aseismic design and non-linear structural analysis of building frames.

Hiroyasu SAKATA
Graduate Student
Tokyo Inst. of Techn.
Tokyo, Japan

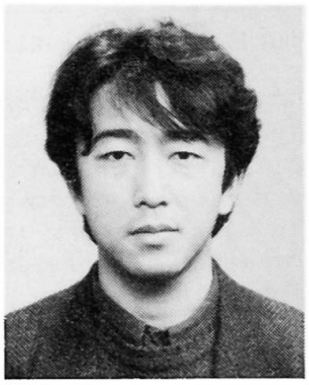

Hiroyasu Sakata, born in 1960, graduated in Building Eng. from Tokyo Inst. of Tech. He received his Master Eng. in 1985 from Tokyo Inst. of Tech.

SUMMARY
This paper presents a method for considering the shear deformation of a beamcolumn joint and the continuity of the reinforcing bars through beams, columns, and beam-column joints. The authors have performed the analyses of a single-storied single-span reinforced concrete structure and a cross-shaped reinforced concrete structure. Analysis results compare favorably with experimental data for these structures.

RÉSUMÉ
L'étude décrit une méthode pour étudier la déformation due au cisaillement d'un joint de poutre-poteau et la continuité des armatures passant par les poutres et poteaux ainsi que les joints poutre-poteau. Les auteurs ont analysé une structure en béton armé à un étage et une portée et une structure en béton armé croisée. Les résultats des analyses correspondent aux données expérimentales.

ZUSAMMENFASSUNG
Die Studie befaßt sich mit einem Verfahren zur Berechnung der Verformung einer Balkenträgerverbindung und der Führung des Bewehrungsstahles durch Balken, Stützen und Rahmenknoten. Von den Autoren wurden Analysen an einem einstöckigen, einschiffigen Stahlbetonrahmen und an einem kreuzförmigen Stahlbetonknoten im Vergleich zu den experimentellen Daten mit guten Ergebnissen durchgeführt.

1. INTRODUCTION

Until now, most analysis methods which consider bond-slip or shear deformation of beam-column joints have been 2-dimensional or 3-dimensional methods, such as finite element method. Some researchers have made use of beam theory taking into consideration shear deformation of beam-column joints[1]. Others have taken into consideration bond-slip[2]-[4]. But there have been few analysis of reinforced concrete frame structures taking into consideration the continuity of reinforcing bars among beam, column and beam-column joints.

In this paper, we report on a technique using finite segment method, that considers the shear deformation of beam-column joints and the continuity of reinforcing bars among beam, column and beam-column joint.

2. ANALYTICAL METHOD

2.1 Modeling of Reinforced Concrete Frame and Analytical Assumptions

An outline of analytical model for a single beam-column joint is shown in Fig.1.

2.1.1 Reinforced concrete members

(a)The member is assumed to be of such type that traditional beam theory is applicable. But in order to approximate the curves of each member after deformation, the member is divided into 20 to 60 member elements.
(b)In each member element, only the bending deformation and the axial deformation is considered and shearing deformation is ignored.
(c)The distribution of stress intensity and strain in the cross section is considered by dividing the cross section into 34 layers as shown in Fig.2. The values of stress and strain in each unit element are represented by the values at the each center point.
(d)Stress and strains condition in member elements are traced solely at the sections at the ends of each member element[5].

2.1.2 Beam-column joints

Beam-column joints are treated as a joint panel. Only shear deformation is considered in the joint panel. In consideration of the bond-slip and yielding of the reinforcement in the joint panel, individual reinforcement in it will be divided into 20 elements in the axial direction of that reinforcement.

2.1.3 Mechanical properties of materials

The stress-strain relation of concrete and reinforcement is taken to follow, hysteresis loops as shown in Fig.3 and Fig.4 respectively. For the bond-slip relation, a hysteresis loop which is shown in Fig.5 is used. For the stress-

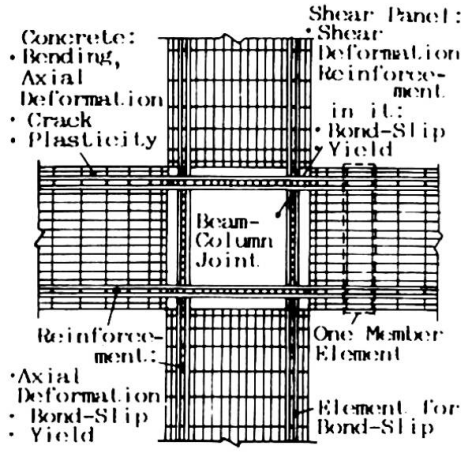

Fig.1 Reinforced concrete frame model

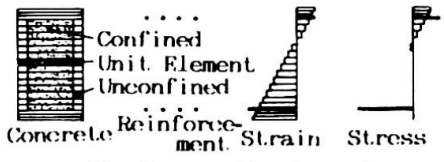

Fig.2 Distribution of strain and stress

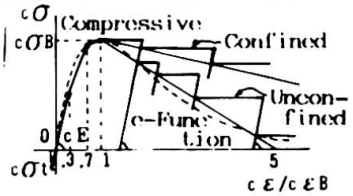

Fig.3 Stress-strain relationship of concrete

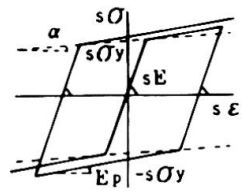

Fig.4 Stress-strain relationship of reinforcement

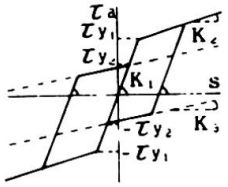

Fig.5 Bond-slip relationship

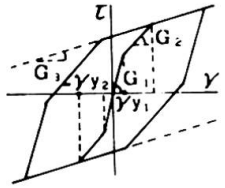

Fig.6 Stress-strain relationship of concrete panel

strain relation of the concrete panel, a hysteresis loop which is shown in Fig.6 is used.

2.1.4 Coordinates and incremental displacements

(a)Axes X and Y in the global coordinate system, and axes x and y in a local coordinate system associated with each of the member elements are defined. Incremental displacements Δu and Δv as the displacement constituents in the directions corresponding to axes x and y, incremental rotation $\Delta\theta$, and the incremental slip of individual reinforcement, Δs, will be considered at individual nodes (Fig.7).

(b)x_p and y_p with the origin positioned at the center of the joint panel are defined. Incremental displacements $\Delta_p u$ and $\Delta_p v$ as the displacement constituents in the directions corresponding to axes x_p and y_p and incremental rotations $\Delta_p\theta_b$ and $\Delta_p\theta_c$ of the beam and column surfaces will be considered at the center points of the joint panel. Regarding individual reinforcement, incremental slips $\Delta_p s$ will be considered at the 19 nodes inside, and the 2 nodes on the surfaces of the ends of the joint panel (Fig.8).

2.2 Analytical Method

The non-linear analytical method discussed in this paper is based on the incremental method, called initial stress method, which is derived from the stationary principle of incremental potential energy. As a result, the equation for each node is given in Eq.(1)

$$K\Delta u + f_{in} - f_{ex} = 0 \qquad \text{— (1)}$$

where K : The whole structure stiffness matrix
Δu : The incremental displacement in the global coordinate system of the whole structure
f_{in} : The internal force vector at the node
f_{ex} : The external force vector at the node

Δu is obtained by using Eq.(1). Then incremental strain in the structure induced by Δu is computed utilizing the local coordinate system at pre-incremental step and also, stress is modified according to such incremental strain. Thus, the computation procedures gain one step.

3. INCREMENTAL DISPLACEMENTS AND INCREMENTAL STRAINS

3.1 Incremental Displacement Inside a Member Element

The cross section which passes through points(x,0) on axis x will be considered. Incremental displacements in the directions corresponding to axes x and y at the points(x,0) on axis x will be taken as Δu and Δv, respectively and incremental rotation displacement will be taken as $\Delta\theta$. Incremental slip between the reinforcement and concrete in tier k within this cross section will be taken as Δs_k (Fig.7).

For concrete elements, the incremental displacements in the directions of x and y at arbitrary points x and y_k within the cross section, and incremental rotation displacements $\Delta_c u$, $\Delta_c v$ and $\Delta_c\theta$ can be expressed as shown in equations (2):

$$\begin{aligned}\Delta_c u &= \Delta u - y\frac{d\Delta u}{dx}\\ \Delta_c v &= \Delta v\\ \Delta_c\theta &= \Delta\theta\end{aligned} \qquad \text{— (2)}$$

For reinforcement x and y in tier k within this cross section, the incremental displacement in the direction of x and the incremental slips $\Delta_s u_k$ and Δs_k between the reinforcement and

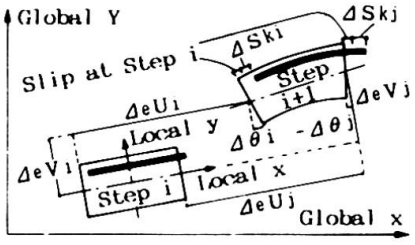

Fig.7 Deformation and coordinate of member element

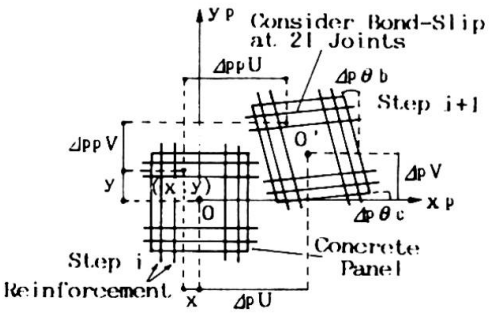

Fig.8 Deformation and coordinate of joint panel

concrete can be as given by eqs.(3) :

$$\begin{aligned} \Delta_s u_k &= \Delta u - y_k \frac{d\,\Delta u}{dx} + \Delta s_k \\ \Delta s_k &= \Delta s_k \end{aligned} \qquad \text{— (3)}$$

3.2 Incremental Shear Strain of A Concrete Panel

It is assumed that the concrete panel is subject to shear deformation only. Incremental shear strain $\Delta\gamma$ in the joint panel can be expressed as the difference between the incremental rotations of column and beam surfaces:

$$\Delta\gamma = \Delta_p\theta_c - \Delta_p\theta_b \qquad \text{— (4)}$$

where $\Delta_p\theta_c$: Incremental rotation of column surface
$\Delta_p\theta_b$: Incremental rotation of beam surface

3.3 Incremental Displacement of Reinforcement in Joint Panel

The incremental displacement $\Delta_{ps}u_b$, in the axial direction of x_p, of the beam reinforcement positioned between axes x_p and y within the joint panel, and the incremental displacement $\Delta_{ps}v_c$, in the axial direction of y_p, of the column reinforcement positioned between axes y_p and x can be expressed as given by equations (5) and (6):

[Beam Reinforcement] $\Delta_{ps}u_b = \Delta_p u - y_p\theta_b + \Delta_p s_b$ — (5)
[Column Reinforcement] $\Delta_{ps}u_c = \Delta_p v - x_p\theta_c + \Delta_p s_c$ — (6)

where $\Delta_p u$: Incremental displacement, in the axial direction of x_p, of the center point of the joint panel
$\Delta_p v$: Incremental displacement, in the axial direction of y_p, of the center point of the joint panel
$\Delta_p s_b$: Incremental slip of beam reinforcement
$\Delta_p s_c$: Incremental slip of column reinforcement

4. COMPATIBILITY OF INCREMENTAL DISPLACEMENTS BETWEEN MEMBER AND JOINT PANEL

The condition of compatibility of incremental displacement at center point P of the joint panel, $\Delta_p u=(\Delta_p u, \Delta_p v, \Delta_p\theta_b, \Delta_p\theta_c)^T$, and that at center point B on the beam surface, $\Delta u_b=(\Delta u_b, \Delta v_b, \Delta\theta_b)^T$, can be expressed as given by eq.(7) (Fig.9). :

$$\begin{bmatrix}\Delta u_b\\ \Delta v_b\\ \Delta\theta_b\end{bmatrix} = \begin{bmatrix}1 & 0 & 0 & 0\\ 0 & 1 & 0 & \ell_x\\ 0 & 0 & 1 & 0\end{bmatrix} \begin{bmatrix}\Delta_p u\\ \Delta_p v\\ \Delta_p\theta_b\\ \Delta_p\theta_c\end{bmatrix} = R_b\,\Delta_p u \qquad \text{— (7)}$$

The condition of compatibility of incremental displacement at center point P of the joint panel, and that at center point C on the column surface, $\Delta u_c=(\Delta u_c, \Delta v_c, \Delta\theta_c)^T$, can be expressed as given by equation (8):

$$\begin{bmatrix}\Delta u_c\\ \Delta v_c\\ \Delta\theta_c\end{bmatrix} = \begin{bmatrix}1 & 0 & -\ell_y & 0\\ 0 & 1 & 0 & 0\\ 0 & 0 & 0 & 1\end{bmatrix} \begin{bmatrix}\Delta_p u\\ \Delta_p v\\ \Delta_p\theta_b\\ \Delta_p\theta_c\end{bmatrix} = R_c\,\Delta_p u \qquad \text{— (8)}$$

where ℓ_x and ℓ_y will be given in the panel coordinate system (see Fig.9).

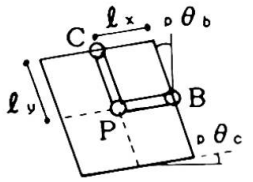

Fig.9 Joint panel

5. COMPARISON OF EXPERIMENTAL AND ANALYTICAL RESULTS

5.1 Single-storied Single-span Reinforced Concrete Structure

Matuzaki and his colleagues experimented with a single-storied single-span reinforced concrete structure. Figure 10 shows the specimen and Fig.11 shows idealized model for the analysis. Tensile force will be applied to the top of the left column when loading in the right direction, and to the top of the right column when loading in the left direction.

Table 1 shows the empirically established mechanical properties of materials and Fig.12 shows both analysis and experimental results for the relationship between load and the horizontal displacement at point ①(see Fig.11). The results of our analysis and agree very well with experimental values. Figure 13 shows the

diagram of deformation at point Ⓐ(P=34.4kN,δ=8.96mm) in Fig.12, the diagram of crack distribution, the diagram of reinforcement stress distribution, and the diagram of bond stress distribution.

Table 1 Mechanical properties

$_cE$	=24892.	MPa	$_sE$ =205800.	MPa
$_c\sigma_B$	=27.2	MPa	E_p =2058.	MPa
$_c\varepsilon_B$	=0.0023		α =1029.	MPa
K_1	=392.	MPa/cm	$_s\sigma_y$ =394.9	MPa
K_2	=19.6	MPa/cm	G_1 =5880.	MPa
K_3	=4.9	MPa/cm	G_2 =4704.	MPa
τ_{y1}	=3.92	MPa	G_3 =1176.	MPa
τ_{y2}	=0.49	MPa	γ_{y1} =0.0005	
			γ_{y2} =0.003	

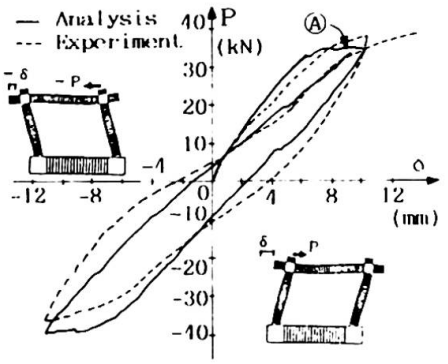

Fig.12 Relation of load-deflection

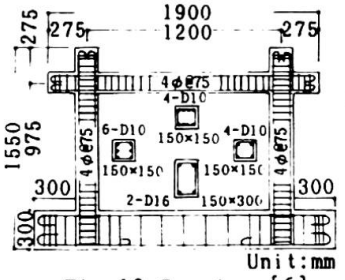

Fig.10 Specimen[6]

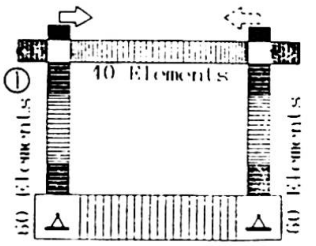

Fig.11 Idealized model for the analysis

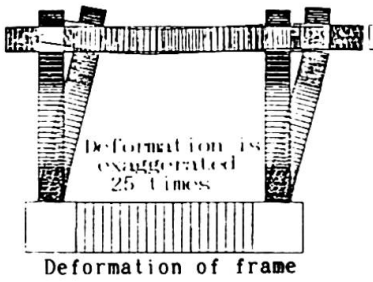

Deformation of frame

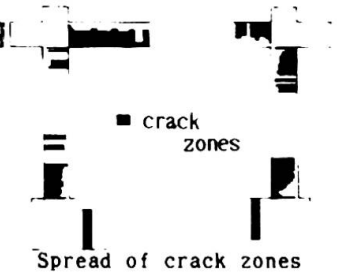

Spread of crack zones

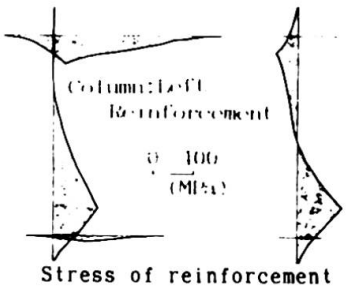

Stress of reinforcement

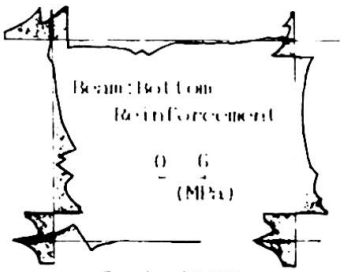

Bond stress

Fig.13 Deformation, crack, reinforcement stress, and bond stress

5.2 Cross-shaped Reinforced Concrete Structure

In another experiment Shirouchi and his colleagues tested a cross-shaped reinforced concrete structure. Figure 14 shows the specimen and Fig.15 shows idealized model for the analysis. Table 2 shows the mechanical properties of materials. Fig.16 shows the relationship between the shearing force of the column and the horizontal displacement at the loading point, where the shearing force is that for which consideration is given to the effect of additional bending moment due to the axial force. Figure 17 shows the relationship between the shearing force of a column and the deflection of a beam derived from the rotation angle of that beam. Figure 18 shows the distribution diagram of beam reinforcement strain. Figure 19 shows the distribution diagram of cracks at point Ⓑ(P=179kN,δ=53.2mm) in Fig.16. The results of experiment and analysis again agree very closely.

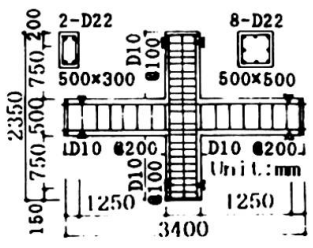

Fig.14 Specimen[7]

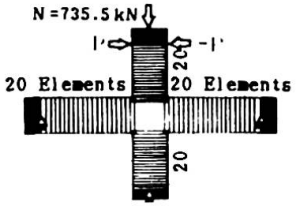

Fig.15 Idealized model for the analysis

Table 2 Mechanical properties

$_cE$	=25578.	MPa	$_sE$ =205800.	MPa
$_c\sigma_B$	=26.6	MPa	E_p =2058.	MPa
$_c\varepsilon_B$	=0.0027		α =1029.	MPa
K_1	=392.	MPa/cm	$_s\sigma_y$ =376.3	MPa
K_2	=19.6	MPa/cm	G_1 =5880.	MPa
K_3	=4.9	MPa/cm	G_2 =4704.	MPa
τ_{y1}	=3.92	MPa	G_3 =1176.	MPa
τ_{y2}	=0.49	MPa	γ_{y1} =0.0005	
			γ_{y2} =0.003	

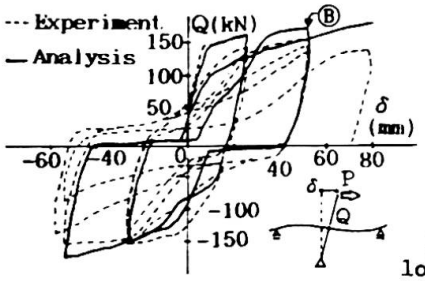

Fig.16 Relation of load-column deflection

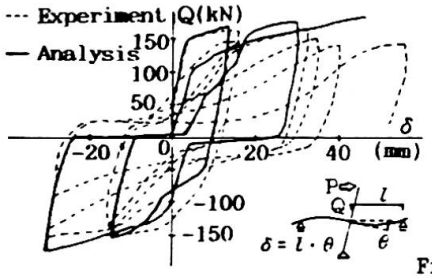

Fig.17 Relation of load-beam deflection

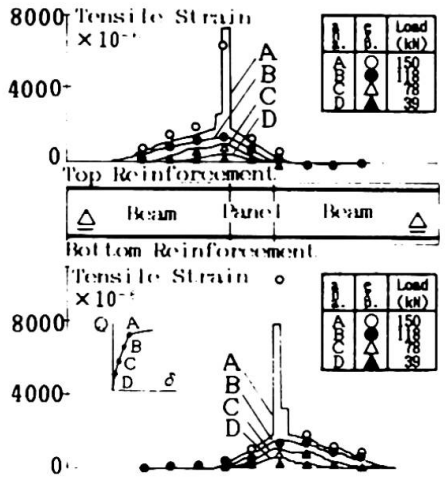

Fig.18 Stress of beam reinforcement

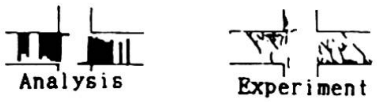

Fig.19 Spread of crack zones

6. CONCLUSIONS

1)By incorporating a joint panel, the shear deformation of beam-column joints can be considered while satisfying the continuity of the reinforcement through the beam-column joints.
2)Although only two analytical examples have been outlined, the results of experiment and analysis show a good correspondence with respect to the load-displacement relationship, reinforcement strain distribution and crack distribution. The analytical method dealt with in this paper would be effective for bending yield type reinforced concrete frames.

7. ACKNOWLEDGMENT

Dr. Yasuhiro Matuzaki, Dr. Shizuo Hayashi and Dr. Katsumi Kobayashi are acknowledged for their constant, useful guidances and provisions of valued experimental data. Messrs. Tetsuo Toda and Akinori Iwasaki, Hazama-Gumi, Ltd. are wholeheartedly acknowledged for permission to use their valued experimental data. Our study gratefully spent part of the grant in aid for scientific research from the Ministry of Education, Science and Culture of Japan, and those concerned are highly acknowledged.

8. REFERENCES

[1] SUGANO T., Analysis Taking into Consideration Shear Deformation of Beam-column Joints using Matrix Method. Sum. of Tech. Papers of Annual Meeting ALJ, Oct. 1968, pp.563-564 (in Japanese).
[2] ICHINOSE T., Method of Inelastic Analysis of Reinforced Concrete Frames with Bond-slip. Trans. of ALJ, No.328, June 1983, pp.26-35 (in Japanese).
[3] TADA T. and TAKEDA T., Analysis of Bond Deterioration Process in Reinforced Concrete Member. Trans. of ALJ, No.351, May 1985, pp.22-30 (in Japanese).
[4] FILIPPOU F.C., POPOV E.P, and BERTERO V.V., Modeling of R/C Joints under Cyclic Excitations. Jour. of Structural Engng., Proc. of ASCE, Vol.109, No.11 Nov. 1983, pp.2666-2684.
[5] WADA A., SUTO F., and FUJIMOTO M., Non-linear Analysis for K-type Braced Steel Frame. IABSE Symposium in Lisbon, September 1973, pp.49-54.
[6] KOKUSHO S., MATUZAKI Y. et al., A Study on Behavior of Deformation of RC Frame under Cyclic Excitations. Trans. of The Kanto Branch of ALJ, 1970, pp.101-104 (in Japanese).
[7] SHIROUCHI T., TODA T. et al., An Experiment on RC Beam-column Joints with Double Sleeve Joint in Reinforcing Bars. Sum. of Tech. Papers of Annual Meeting ALJ, Oct. 1984, pp.1983-1984 (in Japanese).

Dynamic Characteristics of a Liquid Filled Egg-Shaped Tank

Caractéristiques dynamiques d'un réservoir ovoïde plein

Dynamische Einwirkungen einer Flüssigkeit in einem eiförmigen Wassertank

Kiyoshi UNO
Assoc. Prof.
Kyushu Univ.
Fukuoka, Japan

Teruhiko TAKANISHI
Prof. Dr.
Kyushu Inst. of Tech.
Kitakyushu, Japan

Masaru NARITOMI
Dr. Eng.
Kyushu Univ.
Fukuoka, Japan

Seima KOTSUBO
Prof. Dr.
Kyushu Kyoritsu Univ.
Kitakyushu, Japan

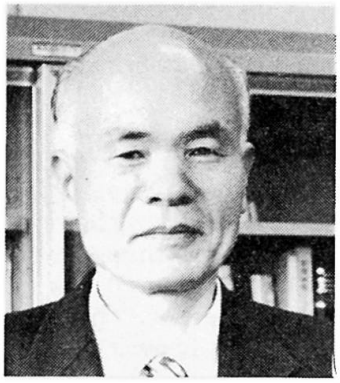

SUMMARY
When an Egg-shaped tank is constructed in Japan, pile-group foundation is used in order to resist the effect of earthquakes. It is difficult to analyse the response of tank, liquid and foundation reaction during earthquakes. We proposed approximate equations for the calculation of dynamic liquid pressures in the Egg-shaped tank during earthquakes.

RÉSUMÉ
La fondation par groupe de pieux est utilisée pour des réservoirs ovoïdes au Japon, afin de résister aux effets des tremblements de terre. Il est difficile d'analyser le comportement du réservoir, du liquide et de la fondation pendant les tremblements de terre. Les auteurs proposent des équations approximatives pour le calcul des pressions dynamiques du liquide dans le réservoir ovoïde lors de séismes.

ZUSAMMENFASSUNG
Beim Bau von eiförmigen Wassertanks wird in Japan zur Aufnahme der Erdbebeneinwirkungen auf Pfahlfundationen zurückgegriffen. Die Berechunung des dyanmischen Verhaltens von Tank, Flüssigkeit und Pfahlgruppe ist relativ schwierig. Es werden Näherungsgleichungen zur Bestimmung der dynamischen Flüssgigkeitsdrücke im eiförmigen Behälter vorgestellt.

1. INTRODUCTION

The Egg-shaped tank shown in Fig.1 is developed in West Germany and it is more effective on sewage purification than that of a cylindrical tank. Recently many tanks of this type have been constructed in West Germany. When the Egg-shaped tank is constructed in Japan, pile-group foundation is used in order to resist the effect of earthquakes, which in turn makes it difficult to analyse the response of the tank, liquid and foundation system subject to earthquakes.

The purpose of this study is to propose the approximate equations for evaluating the dynamic liquid pressures of the Egg-shaped tank during earthquakes. Through the results of this calculation, the value of moment at the top of the pile can be easily obtained.

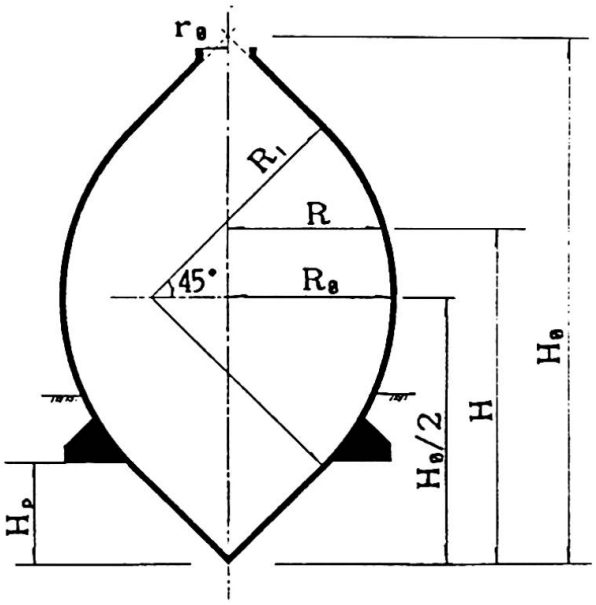

Fig. 1 Egg-shaped tank

2. METHOD OF ANALYSIS

Dimensions of three Egg-shaped tanks constructed in Japan are shown in Table 1. The ratio R_0/H_0 falls in the narrow range between 0.301 and 0.315 for all three cases so that the shapes of these tanks are considered similar to each other. Since the values R_0^3 and $(H_0/2)^3$ are nearly equal to the ratios of volume(V) of each Egg-shaped tank, it is known that the standard of the shape can be set up from the ratio R_0/H_0. H_p is the height from the bottom of the Egg-shaped tank to the top of the pile, as is indicated in Fig.1. Dynamic liquid pressures can be separated into impulsive part, which depends on short period component, and sloshing part which depends on long period component. Since it is difficult to analyse these two types of dynamic liquid pressures exactly, the transfer matrix proposed by Sogabe is used for calculating the dynamic liquid pressures.

Table 1 Dimensions of the Egg-shaped tank

	CASE 1	CASE 2	CASE 3
R_1 (m)	10.600	15.550	13.065
R_0 (m)	6.800	10.900	9.180
r_0 (m)	1.000	2.500	2.495
H_p (m)	4.000	5.000	4.474
$H_0/2$ (m)	11.200	17.340	14.541
R_0/H_0 (m)	0.304	0.314	0.315
V (m^3)	1748.0	6863.0	4000.0

3. RESULTS AND PROPOSED EQUATION

3.1 Impulsive Liquid Pressures (Pi)

Since the value of impulsive liquid pressures increases in proportion to the

acceleration and the height of liquid surface(H), the proposed approximate equations for α_i and H_i/H_0 are written in the following form

$$\alpha_i = 0.27\,(H/H_0) + 0.73 \qquad 0.9 \leqq H/H_0$$
$$= 1.08\,(H/H_0) \qquad 0.5 \leqq H/H_0 < 0.9 \qquad \cdots\cdots\cdots (1)$$

$$H_i/H_0 = 0.25\,(H/H_0) + 0.26 \qquad 0.8 \leqq H/H_0$$
$$= 0.50\,(H/H_0) + 0.06 \qquad 0.5 \leqq H/H_0 < 0.9 \qquad \cdots\cdots\cdots (2)$$

where α_i is the coefficient of added mass and H_i is the height of the loading point of impulsive liquid pressures. Figure 2 shows $\alpha_i - H/H_0$ and $H_i/H_0 - H/H_0$ relationships. Using these values, impulsive liquid pressures(Pi) and the moment(Mi) at the top of the pile can be given as follows

$$P_i = \rho\,\alpha_i\,V_H\,\omega_i^2 A_i \qquad \cdots\cdots\cdots (3)$$

$$M_i = P_i\,(H_i - H_p) \qquad \cdots\cdots\cdots (4)$$

where ρ is the density of liquid, V_H is volume of liquid, ω_i is the natural circular frequency and A_i is amplitude of displacement.

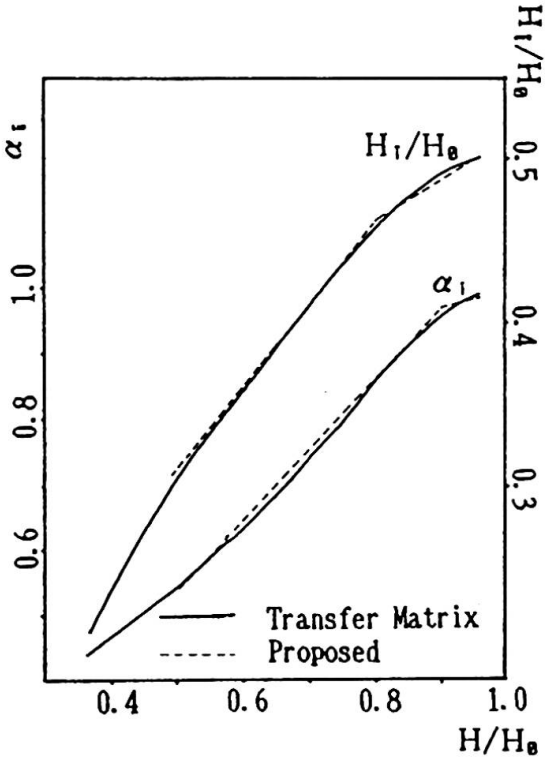

Fig. 2 $\alpha_i - H/H_0$, $H_i/H_0 - H/H_0$ relationships

3.2 Sloshing Liquid Pressures (Ps)

Since sloshing liquid pressures are under the influence of the first vibration mode, the proposed approximate equations are obtained for the first vibratinal mode. The proposed approximate equations for α_s, H_s, T_s, β_s, are written in the following form

$$\alpha_s = 0.37 - 0.40\,(H/H_0)^3 \qquad 0.5 \leqq H/H_0 \qquad \cdots\cdots\cdots (5)$$

$$H_s/H_0 = 0.8\,(H/H_0) \qquad \cdots\cdots\cdots (6)$$

$$T_s/R_0^{0.5} = 1.10\,(R/R_0) + 0.40 \qquad \cdots\cdots\cdots (7)$$

$$\beta_s = 0.27/\{1.0 - (H/H_0) + 0.67\} \qquad \cdots\cdots\cdots (8)$$

where α_s is the coefficient of added mass, H_s is the height of the loading point of sloshing liquid pressures, T_s is the natural period and β_s is the participation factor.

Figure 3 shows α_s — H/H_0 and H_s/H_0 — H/H_0 relationships. $T_s/R_0^{0.5}$ — H/H_0 relationship and β_s — H/H_0 relationship are presented in Fig.4 and Fig.5, respectively.

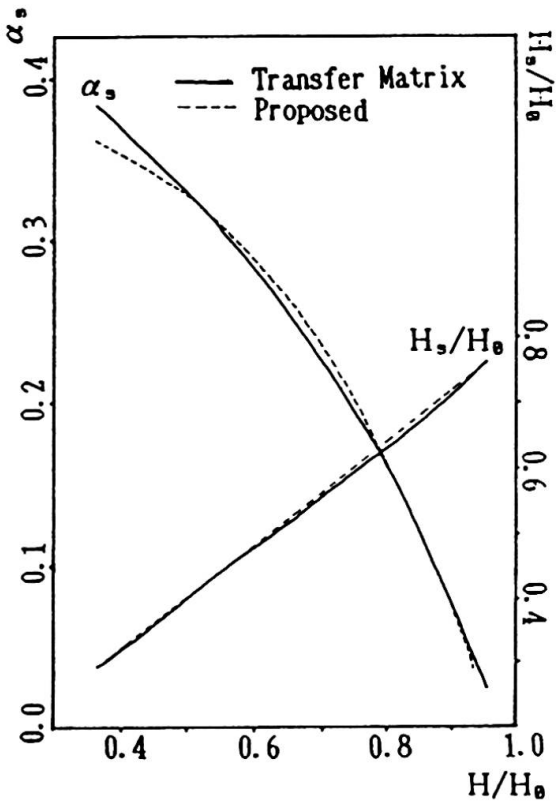

Fig. 3 α_s — H/H_0, H_s/H_0 — H/H_0 relationships

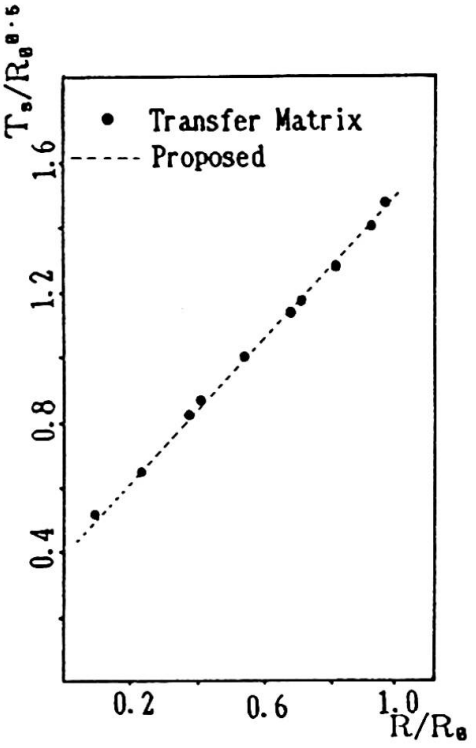

Fig. 4 T_s/R_0 — $R/R_0^{0.5}$ relationships

Using these values, sloshing liquid pressures(Ps), the moment at the top of the pile(Ms) and the maximum vertical displacement of free-surface(Wmax) during earthquakes can be given as follows

$$P_s = \rho \alpha_s V_H \omega_s^2 A_s \quad \cdots\cdots (9)$$

$$M_s = P_s (H_s - H_p) \quad \cdots\cdots (10)$$

$$W_{max} = \beta_s S_A / \omega_s^2 = \beta_s A_s \quad \cdots (11)$$

where ω_s is the natural circular frequency, A_s is the amplitude of earthquake displacement for ω_s and S_A is the amplitude of acceleration for ω_s. Figure 6 shows M_i — H/H_0 and M_s — H/H_0 relationships when the amplitude of input earthquake acceleration is 100 cm/s^2.

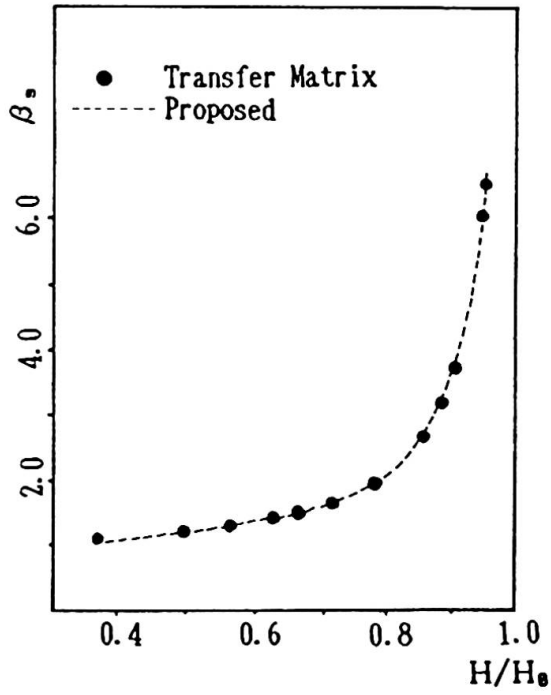

Fig. 5 β_s — H/H_0 relationships relationships

4. CONCLUSIONS

The results are useful for aseismic design of the pile-group foundation. When comparing our proposed results with those of the transfer matrix, the accuracy is quite satisfactory, and the dynamic liquids' characteristics of the Egg-shaped tank can be easily given.

It is essential for aseismic design of the Egg-shaped tank to evaluate the moment at the top of the pile-group foundation. The proposed equations are readily used to estimate this moment.

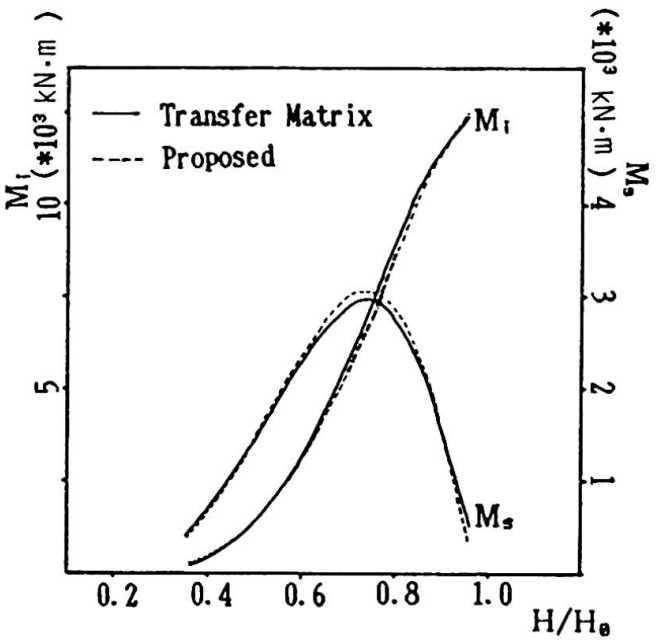

Fig. 6 $M_i - H/H_0$, $M_s - H/H_0$ relationships

REFERENCES

1. Sogabe K., Shigeta T. and Shibata H., A Fundamental Study on the Aseismic Design of Liquid Storages, Report of the Institute of Industrial Science, March 1977.

2. Abramson,H.N. ed., The Dynamic Behavier of Liquids in Moving Containers, with Applications to Space Vehicle Technology, NASA SP-106 1966.

3. Housner,G.W., Dynamic Pressures on Accelerated Fluid Containers, Bulletin of the Seismological Society of America Vol.47, No.1, 1957.

4. Graham,E.W. and Rodriguez,A.M., The Characteristics of Feul Motion Which Affect Airplane Dynamic, Journal of Applied Mechanics, Vol.19, No.3, September 1952.

5. Cambra,F.J., Earthquake Response Considerations of Broad Liquid Storage Tnaks, University of California Earthquake Engineering Research Center Report Number UCB/EERC-82/25, November 1982.

6. Budiansky,B., Sloshing of liquids in Circular Canals and Spherical Tanks, Journal of the Aero Space Sciences, Vol.27, No.3, March 1960.

7. Dokuchaev,L.V., On the Solution of a Boundary Value Problem on the Sloshing of a Liquid in Conical Cavities, Journal of Applied Mathmatics and Mechanics(PMM), Vol.28, No.1, 1964.

8. Nakayama T., and Washizu K., Nonlinear Analysis of Liquid Motion in a Container Subjected to Forced Pitching Oscillation, International Journal for Numerical Methods in Engineering, Vol.15, 1207-1220, 1980.

9. Aslam,M., Finite Element Analysis of Earthquake Induced Sloshing in Axisymmetric Tanks, International Journal for Numerical Methods in Engineering, Vol.17, 159-170, 1981.

10. Liu,W.K. and Ma,D.C., Coupling Effect Between Liquid Sloshing and Flexible Fluid-Filled Systems, Nuclear Engineering and Design, Vol.72, 345-357, 1982.

11. Abramson,H.N., Dynamic Behavier of Liquid in Moving Container, Applied Mechanics Review, Vol.16, No.7, July 1963.

Leere Seite
Blank page
Page vide

Leere Seite
Blank page
Page vide